

Rendering and Extracting Extremal Features in 3D Fields

1279

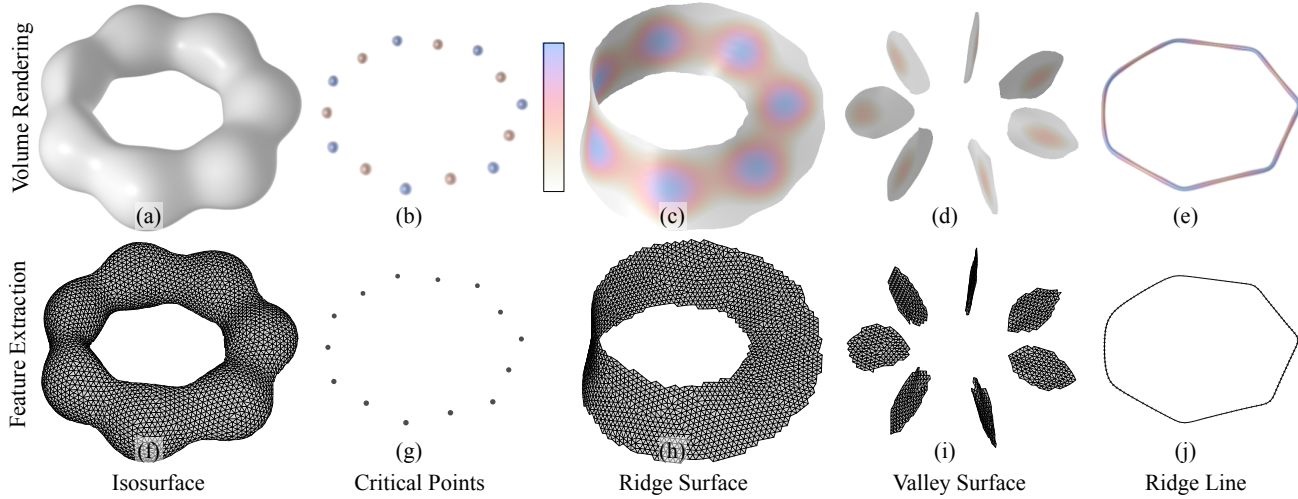


Figure 1: Direct volume renderings (top row) and meshes (bottom row) show the structure of one synthetic dataset. One program computed all renderings, and another computed the mesh vertices. Between features (columns), the only differences in their source code were functions for computing a Newton step to the feature, and for measuring feature strength. These functions were shared between the two programs, achieving orthogonality between implementing visualization algorithms, and specifying the particular features of interest.

Abstract

Visualizing and extracting features of interest from three-dimensional data lies at the heart of virtually all computational sciences. Consequently, there exist a plethora of feature definitions for different data types and different applications. While some of these are simple to state and implement, i.e. isosurfaces, others involve multiple derivatives, complex derived fields like curvature, eigenvectors, etc. Especially for vector- and tensor-valued data, implementing these mathematical concepts is difficult and experimenting with new definitions requires substantial investments. Furthermore, traditional interpolants rarely support the necessary derivatives and the various approximations make solutions numerically unstable and delicate to implement.

We introduce a new framework that directly translates mathematical notation into practical visualization and feature extraction. Using higher-order smooth interpolants and an appropriate choice of domain specific language, we compute direct volume rendering and particle-based feature sampling and extraction from a wide range of mathematical definitions with minimal mental and implementation overheads. This, for the first time, enables non-expert users to experiment with and improve complex feature definitions without any exposure to meshes, interpolants, derivative computation, etc. We demonstrate the power of our approach by providing high-quality results on notoriously difficult features, such as ridges and vortex cores, using working code simple enough to be presented in its entirety.

CCS Concepts

- Computing methodologies → Scientific visualization; • Software and its engineering → Domain specific languages;
- Human-centered computing → Visualization systems and tools;

1. Introduction

While there are many different analysis and visualization techniques for spatio-temporal data, virtually all aim for the same over-

arching goal: to better understand some feature of interest. Features may be defined using *local* conditions, i.e. isosurfaces as points with a certain value, edges as points with strong gradients, or *glob-*

ally, i.e. streamlines, separatrices, etc. In general, local feature definitions are more common and cover features ranging from isosurfaces and ridges in scalar fields [Ebe96], to vortex core lines in vector fields [PR99] and crease lines in tensor fields [TKW08]. Depending on the application, these definitions are either approximated by some (potentially fuzzy) indicator, such as, a transfer function in volume rendering or explicitly evaluated through an algorithm like Marching Cubes [LC87]. However, feature definitions studied in visualization research have long evolved from the simple definitions (like that of isosurfaces) to complex, often multi-variate expressions that involve higher order derivatives, curvatures, Jacobians and any number of mathematical expressions not easily build from scratch. Furthermore, the common bi- or trilinear interpolation schemes do not provide continuous derivatives of any order. Therefore, applying any more advanced feature definition typically requires various approximations and often leads to numerical instabilities and significant artifacts.

A typical example is ridge extraction: Ridges are commonly defined using a concisely expressed local indicator that, however, involves eigenvectors of the Hessian matrix [Ebe96]. The resulting indicator computed through stencil computations is known to be numerically unstable, often produces false positives and typically requires some amount of pre-smoothing to be effective [SP07, PS08]. Finally, even if higher order interpolation schemes are available [NLKH12, NKH13] generalizing many of the traditional algorithms has proven challenging.

Our new approach allows users to easily express complex feature definitions directly in common mathematical notation. Given sampled data and a sufficiently smooth reconstruction, these expressions produce computationally tractable methods of visualization and extraction. Since all derivative and tensor evaluations are performed analytically, our feature definitions do not suffer from the common discretization artifacts. Most importantly, the complexity and implementation details of advanced feature definitions are hidden from the user: experimenting with new definitions is more akin to copying mathematical definitions into code, rather than bearing the traditional per-feature and per-application implementation costs. Our approach directly applies to a wide range of use cases and simplifies handling challenging problems previously addressed with complex, dedicated solutions.

The two main contributions of this work are (1) conceptually bridging direct volume rendering of features with their explicit geometric extraction, and (2) implementing both in a way that is general with respect to feature type and application. We start with standard mathematical feature definitions (one or more equations satisfied at points *within* the feature, e.g. $\{\mathbf{x} | f(\mathbf{x}) = v_0\}$ for isosurfaces), but we employ a *feature step* function that describes one step *towards* the feature (e.g. the Newton-Raphson step $\frac{(v_0 - f(\mathbf{x})) \nabla f(\mathbf{x})}{\nabla f(\mathbf{x}) \cdot \nabla f(\mathbf{x})}$ for isosurfaces). The same feature step function can either be evaluated once to define a transfer function for direct volume rendering features, or evaluated repeatedly by particles uniformly sampling a feature. Code for rendering and extracting features is made specific to the feature, and to the application of interest, by choosing the step function for that feature, and defining the field in which the feature is sought. Our initial work focuses on *extremal features*, a class of features wherein some scalar is at an

extremum with respect motion within a locally defined constraint space [TM98, AK04]. Fig. 1 illustrates our approach with isosurfaces and a variety of extremal features (ridges, valleys, and critical points). The implementation of these visualizations enjoys a clean separation between feature-specific code (shared between the volume rendering and particle-based feature sampling programs) versus algorithm-specific code (which was otherwise unchanged across the different features). Our approach is enabled by using a programming language, Diderot, with the necessary mathematical expressivity [Chi17, CKR*12, KCS*16].

2. Mathematical Background

Our method is based on Taylor expansions. For isosurfaces, we review in Sec. 2.1 how a first-order Taylor expansion generates the formula for one iteration of Newton-Raphson root finding, which we term the *feature step* function $s(\mathbf{x})$. We note that the isosurface feature step function leads to Levoy's bivariate transfer function for displaying isocontours [Lev88]. We then develop formulae for feature step functions for ridges and valleys. After defining what we mean by "extremal feature", Sec. 2.2 extends this to other extremal features of interest. Sec. 2.3 then formulates functions for *feature strength* to filter out insignificant features, and we note a connection to previous criteria for filtering ridge pixels [Har83].

2.1. Basic Feature Step Functions, and Shading

The 1st-order Taylor expansion of scalar field f around \mathbf{x} is

$$f(\mathbf{x} + \boldsymbol{\epsilon}) \approx f(\mathbf{x}) + \nabla f(\mathbf{x}) \cdot \boldsymbol{\epsilon} \quad (1)$$

If we assume $f(\mathbf{x} + \boldsymbol{\epsilon}) = v_0$ for some isovalue of interest v_0 , then (1) describes a condition on the possible offsets $\boldsymbol{\epsilon}$ from \mathbf{x} to a point $\mathbf{x} + \boldsymbol{\epsilon}$ on the v_0 isocontour. We can choose an offset $\boldsymbol{\epsilon} = \ell \frac{\nabla f(\mathbf{x})}{|\nabla f(\mathbf{x})|}$ parallel to the gradient $\nabla f(\mathbf{x})$, and then solve for ℓ to arrive at a formula for the feature step function for isosurfaces:

$$v_0 - f(\mathbf{x}) \approx \nabla f(\mathbf{x}) \cdot \boldsymbol{\epsilon} = \nabla f(\mathbf{x}) \cdot \ell \frac{\nabla f(\mathbf{x})}{|\nabla f(\mathbf{x})|} = \ell |\nabla f(\mathbf{x})| \quad (2)$$

$$\Rightarrow \ell = \frac{v_0 - f(\mathbf{x})}{|\nabla f(\mathbf{x})|} \Rightarrow s_{\text{iso}}(\mathbf{x}) = \frac{(v_0 - f(\mathbf{x})) \nabla f(\mathbf{x})}{\nabla f(\mathbf{x}) \cdot \nabla f(\mathbf{x})}. \quad (3)$$

For locations \mathbf{x} near isocontour $f(\mathbf{x}) = v_0$, $s_{\text{iso}}(\mathbf{x})$ (3) indicates the distance and direction towards the feature.

To volume render, we assign opacity with a tent function parameterized by distance d to an isocontour of interest

$$\alpha_{\text{tent}}(d) = \alpha_0 \max \left(0, 1 - \frac{|d|}{w} \right), \quad (4)$$

where w is the full-width half-max of $\alpha_{\text{tent}}(d)$, the apparent thickness of the rendered isocontour. Plugging (3) into (4):

$$\alpha(\mathbf{x}) = \alpha_{\text{tent}}(|s_{\text{iso}}(\mathbf{x})|) = \alpha_0 \max \left(0, 1 - \frac{1}{w} \frac{|v_0 - f(\mathbf{x})|}{|\nabla f(\mathbf{x})|} \right). \quad (5)$$

Eq. (5) is exactly Levoy's bivariate opacity function for rendering approximately constant-thickness isocontours, which he justifies with assumptions equivalent to (1); c.f. Eq. 3 in [Lev88].

Feature step functions also facilitate building geometric models

of features. Locations of model vertices may be found by iterated application of the feature step function

$$\mathbf{x}_{i+1} = \mathbf{x}_i + \mathbf{s}(\mathbf{x}_i), \quad (6)$$

combined with some strategy (such as mutual repulsion) for uniformly distributing points across the feature. This Newton-based approach has been used widely for sampling implicit surfaces [WH94, CA97, CHJ03, LHR05, MGW05].

The above treatment of isocontours exemplifies our approach. A feature step formula may be derived from the Taylor expansion around the feature of interest, such as the extremal features explored here. Then, the same feature step function can be plugged into either the opacity function of a volume render to display the feature, or into the constraint satisfaction of an interacting particle system to explicitly sample the feature. Programs for feature visualization or extraction become specific to the feature via the feature step function. We now derive feature step functions $\mathbf{s}(\mathbf{x})$ for various extremal features of interest.

Newton-Raphson optimization, to find critical points \mathbf{x} where $\nabla f(\mathbf{x}) = \mathbf{0}$, is also based on Taylor expansion. Differentiating (1) with respect to \mathbf{x} produces

$$\nabla f(\mathbf{x} + \boldsymbol{\epsilon}) \approx \nabla f(\mathbf{x}) + \mathbf{H}f(\mathbf{x})\boldsymbol{\epsilon}, \quad (7)$$

where $\mathbf{H}f(\mathbf{x})$ is the Hessian (second derivative) of f at \mathbf{x} . Assuming $\mathbf{x} + \boldsymbol{\epsilon}$ is a critical point (that is, $\nabla f(\mathbf{x} + \boldsymbol{\epsilon}) = \mathbf{0}$), then

$$-\nabla f(\mathbf{x}) \approx \mathbf{H}f(\mathbf{x})\boldsymbol{\epsilon} \Rightarrow \mathbf{s}_{cp}(\mathbf{x}) = -(\mathbf{H}f(\mathbf{x}))^{-1}\nabla f(\mathbf{x}). \quad (8)$$

The signs of Hessian eigenvalues determine the type of the critical point (minima, maxima, or saddle point).

We use Eberly's definitions of ridge (and valley) surfaces and lines [Ebe96] to define their feature step formulae. The Hessian $\mathbf{H}f(\mathbf{x})$ at \mathbf{x} has sorted real eigenvalues $\lambda_0 \geq \lambda_1 \geq \lambda_2$ and corresponding unit-length and mutually orthogonal eigenvectors $\mathbf{e}_0, \mathbf{e}_1, \mathbf{e}_2$. Point \mathbf{x} is on a ridge surface if f is maximal at \mathbf{x} with respect to motion along eigenvector \mathbf{e}_2 (corresponding with the most negative eigenvalue λ_2), i.e. $\nabla f(\mathbf{x}) \cdot \mathbf{e}_2 = 0$ and $\lambda_2 < 0$. Ridge line membership is defined by $\nabla f(\mathbf{x}) \cdot \mathbf{e}_1 = \nabla f(\mathbf{x}) \cdot \mathbf{e}_2 = 0$ and $\lambda_1 < 0$. Ridge and valley features can be uniformly treated by defining a projection \mathbf{P} onto the span of one or two eigenvectors, with

$$\begin{aligned} \mathbf{P}_{rs} &= \mathbf{e}_2 \otimes \mathbf{e}_2, & \mathbf{P}_{rl} &= \mathbf{e}_1 \otimes \mathbf{e}_1 + \mathbf{e}_2 \otimes \mathbf{e}_2, \\ \mathbf{P}_{vs} &= \mathbf{e}_0 \otimes \mathbf{e}_0, & \mathbf{P}_{vl} &= \mathbf{e}_0 \otimes \mathbf{e}_0 + \mathbf{e}_1 \otimes \mathbf{e}_1, \end{aligned} \quad (9)$$

for ridge surfaces (rs) and lines (rl), and valley surfaces (vs) and lines (vl). Left-multiplying both sides of (7) by \mathbf{P} gives

$$\mathbf{P}\nabla f(\mathbf{x} + \boldsymbol{\epsilon}) \approx \mathbf{P}\nabla f(\mathbf{x}) + \mathbf{P}\mathbf{H}f(\mathbf{x})\boldsymbol{\epsilon}. \quad (10)$$

Ridge/valley feature membership of $\mathbf{x} + \boldsymbol{\epsilon}$ implies $\mathbf{P}\nabla f(\mathbf{x} + \boldsymbol{\epsilon}) = \mathbf{0}$, i.e. $f(\mathbf{x} + \boldsymbol{\epsilon})$ is at an extremum with respect to motion within the range of \mathbf{P} . \mathbf{P} and $\mathbf{H}f(\mathbf{x})$ commute since they are both diagonal in the eigenvector basis. Analogous to how in (1) we chose $\boldsymbol{\epsilon}$ parallel to ∇f to derive \mathbf{s}_{iso} (3), in (10) we chose to align $\boldsymbol{\epsilon}$ with relevant Hessian eigenvectors: $\mathbf{P}\boldsymbol{\epsilon} = \boldsymbol{\epsilon}$. These simplifications to (10) give

$$-\mathbf{P}\nabla f(\mathbf{x}) = \mathbf{H}f(\mathbf{x})\boldsymbol{\epsilon} \quad (11)$$

$$\Rightarrow \mathbf{s}_{ft}(\mathbf{x}) = -(\mathbf{H}f(\mathbf{x}))^{-1}\mathbf{P}_{ft}\nabla f(\mathbf{x}), \quad (12)$$

where feature type "ft" can be rs, rl, vs, or vl (c.f. 9). Since \mathbf{P}

depends on the Hessian \mathbf{H} eigensystem, its product (12) with the Hessian inverse can be simplified. With ridge surfaces, for example,

$$\mathbf{s}_{rs}(\mathbf{x}) = -(\mathbf{H}f(\mathbf{x}))^{-1}\mathbf{P}_{rs}\nabla f(\mathbf{x}) = -\frac{\mathbf{e}_2(\mathbf{e}_2 \cdot \nabla f(\mathbf{x}))}{\lambda_2}. \quad (13)$$

Obermaier et al. used (13) for ridge surface sampling [OMD*12]. If multiple iterations of (12) converge to a location \mathbf{x} , tests on eigenvalue signs at \mathbf{x} can verify membership in the desired ridge/valley feature.

Besides assigning opacity, direct volume rendering uses shading to convey surface orientation and shape. The codimension-one and codimension-two features considered above have analytically defined normals and tangents, respectively, that can be used for shading. In the current work, we explore using the step function $\mathbf{s}(\mathbf{x})$ itself for shading, based on an *approximate* surface normal $-\mathbf{s}(\mathbf{x})/|\mathbf{s}(\mathbf{x})|$. For isocontours, this will give the correct shading, but it is not correct for ridge and valley features; normals and tangents for those features depend on third derivatives [Ebe96]. In addition, ridges may be non-orientable surfaces, with no globally consistent orientation [STS10]. We employ two-sided lighting as a simple approach that works adequately for all features.

2.2. Other Extremal Features

The ridges and valleys in the previous section are examples of the extremal features we consider. The terminology of "extremal features" has been used in different ways. In the context of flow field analysis, Sahner et al. use "extremal features" to refer to topological separatrices of strain (as a scalar field); these features are defined globally rather locally, as we do [SWTH07]. In tensor field analysis, Zobel and Scheuermann use "extremal features" to refer to points in the field with a non-invertible tangent space map from the field domain to the 3D space of invariants [ZS17], which is a more general consideration of extrema that we attempt here. Following the earlier terminology of Guy and Medioni [GM97], Tang and Medioni [TM98], and Amenta and Kil [AK04], we consider *extremal features to be the extrema of some scalar field with respect to motion within a locally defined constraint space*. Critical points lack a constraint space (or rather the constraint space is the same as the field domain). For ridges and valleys, the constraint space is spanned by one or more Hessian eigenvectors. Ridges and valleys include not only features of scalar fields reconstructed from scalar data, but also ridges and valleys of the scalar invariants of the Jacobian of a vector field (for flow analysis), and of the invariants in a tensor field; these are explored in Sec. 4.

To define the feature step function for extremal *surfaces*, let \mathbf{c} be the unit-length direction along which the extremum of scalar f is sought (to make $\nabla f \cdot \mathbf{c} = 0$). A Newton optimization step along \mathbf{c} at \mathbf{x} is then

$$f' = \nabla f \cdot \mathbf{c}; \quad f'' = \mathbf{c} \cdot (\nabla \otimes \nabla f)\mathbf{c} \quad (14)$$

$$\mathbf{s}_{-s}(\mathbf{x}) = \mathbf{s}_{+s}(\mathbf{x}) = -\frac{f'}{f''}\mathbf{c} \quad (15)$$

where subscripts " $-s$ " and " $+s$ " indicate minimal and maximal surfaces, respectively; the same Newton step applies to both; a test of f'' will determine the kind of extremum that iterations of (15) converged to.

For extremal *lines*, let $\mathbf{c}_0, \mathbf{c}_1$ span the plane within which the extrema of f is sought (to make $\nabla f \cdot \mathbf{c}_0 = \nabla f \cdot \mathbf{c}_1 = 0$), and let g and H be the projection of the gradient ∇f and Hessian $\mathbf{H} = \nabla \otimes \nabla f$, respectively, onto that plane:

$$g = \begin{bmatrix} \mathbf{c}_0 \cdot \nabla f \\ \mathbf{c}_1 \cdot \nabla f \end{bmatrix}; \quad H = \begin{bmatrix} \mathbf{c}_0 \cdot \mathbf{Hc}_0 & \mathbf{c}_0 \cdot \mathbf{Hc}_1 \\ \mathbf{c}_1 \cdot \mathbf{Hc}_0 & \mathbf{c}_1 \cdot \mathbf{Hc}_1 \end{bmatrix}. \quad (16)$$

Whether seeking the local maxima or minima of f restricted to the span of $\{\mathbf{c}_0, \mathbf{c}_1\}$, (to find maximal line or minimal line features, respectively), we expand the 2D Newton step in the $\{\mathbf{c}_0, \mathbf{c}_1\}$ basis:

$$\mathbf{s} = \begin{bmatrix} s_0 \\ s_1 \end{bmatrix} = -H^{-1}(\mathbf{x})g(\mathbf{x}) \quad (17)$$

$$\mathbf{s}_{-\ell}(\mathbf{x}) = \mathbf{s}_{+\ell}(\mathbf{x}) = s_0 \mathbf{c}_0 + s_1 \mathbf{c}_1 \quad (18)$$

where subscripts “ $-\ell$ ” and “ $+\ell$ ” indicate minimal and maximal lines, respectively.

We can also consider the intersection of two kinds of features, such as isosurfaces and extremal surfaces. *Surface creases* are an example of this. Recall if a surface normal map is $\nabla \otimes \mathbf{n}$, so that

$$\mathbf{n}(\mathbf{x} + \boldsymbol{\epsilon}) \approx \mathbf{n}(\mathbf{x}) + (\nabla \otimes \mathbf{n})\boldsymbol{\epsilon} \quad (19)$$

describes local change in surface normal \mathbf{n} around \mathbf{x} for offsets $\boldsymbol{\epsilon}$ tangent to the surface ($\boldsymbol{\epsilon} \cdot \mathbf{n} = 0$), then curvature along unit-length tangent direction \mathbf{d} is [Car76]

$$\kappa(\mathbf{d}) = \mathbf{d} \cdot (\nabla \otimes \mathbf{n})\mathbf{d}. \quad (20)$$

Curvature is extremal along the *curvature directions* \mathbf{d}_1 and \mathbf{d}_2 , with *principal curvatures* $\kappa_1 = \kappa(\mathbf{d}_1)$ and $\kappa_2 = \kappa(\mathbf{d}_2)$, in that $\kappa_1 \geq \kappa_2$ and curvature $\kappa(\mathbf{d})$ for any other direction \mathbf{d} is within $[\kappa_2, \kappa_1]$. Considering the local variation $\nabla \kappa_1, \nabla \kappa_2$ of the principal curvatures, surface creases are at points \mathbf{x} where $\nabla \kappa_1 \cdot \mathbf{d}_1 = 0, \kappa_1 > 0$ (outward creases) and $\nabla \kappa_2 \cdot \mathbf{d}_2 = 0, \kappa_2 < 0$ (inward creases), i.e., a principal curvature is extremal with respect motion along the corresponding curvature direction [Koe90]. In the context of volumetric image analysis, these have been called *crest lines* [MLD94, MB95]. Crease lines are the intersection of an implicit surface with a curvature extremum surface. Despite their potential for highlighting salient portions of surfaces, surface crease lines have not enjoyed widespread study to date, perhaps because of the third derivatives required (derivatives of curvature, which is itself based on second derivatives) and the resulting formulaic complexity.

2.3. Feature Strength and Mask Functions

Features are worth visualizing or extracting insofar as they indicate the presence and shape of some underlying structure of interest, rather than artifacts or noise in the background. To complement the feature step function that points towards the feature, we also use *feature strength* functions to render or extract only those portions of features that exceed some user-defined significance or strength threshold. Formulating feature strength and specifying strength thresholds are unfortunately not as clear-cut as deriving step functions from feature definitions. For isosurfaces, simply testing for non-zero gradient magnitude may be sufficient, since that ensures the feature step is finite, even though does not indicate feature strength per se.

Work on ridge features has produced more complex feature strength functions. Following Haralick [Har83], Schultz et al. [STS10] test whether $|\nabla f|/\lambda_2$ (in our notation) is *below* a threshold to judge the significance of a point on a ridge surface. Comparing to the feature step function for ridge surfaces (13), we note that when ∇f is parallel to eigenvector \mathbf{e}_2 , this is equivalent to testing for small feature step length $|s_{rs}|$, but it more generally penalizes a large gradient component orthogonal to the step direction. We develop a function that is *large* for “strong” ridge surface features by considering the negated reciprocal of the indicator used by Haralick and Schultz et al., $-\lambda_2/|\nabla f|$, which is large when λ_2 is very negative (the height is clearly concave-down when cutting across the ridge) and $|\nabla f|$ is small (the ridge does not run along the gradient of a steep hill). To gracefully handle $|\nabla f| \approx 0$ and to provide additional control over what downward concavity should be deemed significant, we propose these strength measures for ridge and valley surfaces and lines:

$$\begin{aligned} \mathbf{r}_{rs} &= \frac{-\lambda_2}{r_0 + |\nabla f|}, & \mathbf{r}_{rl} &= \frac{-\lambda_1}{r_0 + |\nabla f|}, \\ \mathbf{r}_{vs} &= \frac{\lambda_0}{r_0 + |\nabla f|}, & \mathbf{r}_{vl} &= \frac{\lambda_1}{r_0 + |\nabla f|}, \end{aligned} \quad (21)$$

where rs, rl, vs , and vl mean the same as in (9), and $r_0 > 0$ is the *feature strength bias*. For a fixed feature strength threshold (which we assume is positive), increasing the bias r_0 creates a more stringent test on the negative magnitude (for ridges) or positive magnitude (for valleys) of the eigenvalue relevant for the feature.

We adapt the above strength measure for other extremal features not defined in terms of Hessian eigenvectors.

$$\mathbf{r}_{-s} = \frac{f''}{r_0 + |\nabla f|}, \quad \mathbf{r}_{+s} = \frac{-f''}{r_0 + |\nabla f|}, \quad (22)$$

where \mathbf{c} is the direction (as above) along which the extremum is sought, and $f'' = \mathbf{c} \cdot (\nabla \otimes \nabla f)\mathbf{c}$ is the second directional derivative of f along \mathbf{c} . For extremal lines, again consider H (16), the Hessian of f projected to the plane within which the extremum is sought. We then propose strength measures for minimal line (“ $-\ell$ ”) and maximal line (“ $+\ell$ ”) features:

$$\mathbf{r}_{-\ell} = \frac{\rho_0}{r_0 + |\nabla f|}, \quad \mathbf{r}_{+\ell} = \frac{-\rho_1}{r_0 + |\nabla f|}, \quad (23)$$

where $\rho_0 \geq \rho_1$ are the eigenvalues of H .

It may be useful to have other controls for including or excluding some part of the feature in addition to the strength measures. For example, one might require that ridges not only have sufficient strength but also sufficient height. In particular, when extracting Sujudi-Haines vortex cores [SH94] by the Parallel Vectors operator with ridge or valley lines of $h = (\mathbf{v}/|\mathbf{v}|) \cdot (\nabla \otimes \mathbf{v}/|\nabla \otimes \mathbf{v}|)$, we want h to be near ± 1 . We include in our approach an additional *feature mask* function that may be set and thresholded to afford this extra control as needed.

3. Methods

We chose to implement our approach in Diderot, a domain-specific language for scientific visualization [Chi17, CKR*12, KCS*16]. Its mathematical syntax, which includes ∇ for differentiation, \otimes for tensor product, and \bullet for inner product, combined with the ability

to apply operators to fields (to produce, for example, a scalar field of curvature), allows directly expressing the fields and features of Sec. 2 in code. In addition, its parallel execution (via pthreads) facilitates work with real datasets (the open-source “vis15” branch we used lacks GPU support). We describe two Diderot programs, one for volume rendering (Sec. 3.1) and one for particle-based feature sampling (Sec. 3.2), and describe how each may be specialized with feature functions. Code for the features functions is listed in the context of volume rendering, but then re-used verbatim for particle-based feature sampling.

3.1. Direct Volume Rendering

The program in Fig. 2 volume renders isosurfaces and demonstrates the basic structure of Diderot programs. Input variables (lines 1–8) include rendering parameters, the isovalue, and the image data from which the C^2 -continuous field F is created by convolving with the cubic B-spline (line 9). After computing ray and camera geometry (lines 14–18), the `atent` function (line 20) implements a modified $\alpha_{\text{tent}}(d)$ (4), parameterized by isosurface thickness `thick`. The ray strand (the unit of parallelism in Diderot) starting line 22 renders one ray. After computing ray geometry (lines 23–26), lines 27–30 initialize ray state, and the `update` method (starting line 31) implements one iteration of ray traversal and volume sampling, as explained in the code comments. The program ends (line 50) by creating an array of strands to be executed in parallel. Figure 3a shows how this program rendered a small $64 \times 64 \times 32$ synthetic dataset (used throughout this section) containing a Möbius strip with seven Gaussian blobs along its circular core.

The Fig. 2 renderer demonstrates how feature specificity can be isolated to a few functions, in this case feature step `fStep` and feature strength `fStrength`, on lines 11 and 12. The `fStep(x)` function, directly copied from `s(x)` (3) of Sec. 2, determines opacity (line 43) and shading (line 45) based on `step = fStep(pos)` (line 42). The `fStrength(pos)` function (line 39) is used here to avoid divide-by-zero problems when computing feature steps; it will have a greater role in other features (such as ridges), where low-strength features correspond to noise or artifacts apart from the underlying objects of interest. With different feature functions, the same program could be used to render different features.

Results in Sec. 4 come from a more complete volume renderer, listed in Appendix A. Compared to Fig. 2, this program renders in color (with a univariate colormap of the underlying scalar value) and it offers more control over ray geometry and rendered appearance, but it too hinges on the same `fStep` and `fStrength` functions. The top row of Fig. 1 shows a variety of features all volume rendered from the same Möbius strip synthetic dataset used in Fig. 3a, all created with the program in Appendix A (used without change for Fig. 1a). Copying (8) from Sec. 2, we can change `fStep` and `fStrength` to show critical points instead:

```
function vec3 fStep(vec3 x) = // critical points
    -inv( $\nabla \otimes \nabla F(x)$ ) •  $\nabla F(x)$ ;
function real fStrength(vec3 x) = | $\nabla \otimes \nabla F(x)$ |;
```

This produces in Fig. 1b. The image clarity benefits from `fStrength` (the Frobenius norm of the Hessian) and a user-defined threshold to give opacity only to critical points near significant second-order variation. Direct volume rendering offers visual

feedback to help determine such thresholds. For consistency one colormap of scalar data value is used for all renderings in Fig. 1, which for this synthetic dataset clearly distinguishes in Fig. 1(b) between maxima (blue) and saddle points (orange). Hessian eigenvalues could also be used to distinguish the critical point types.

Rendering ridges requires the Hessian eigensystem. The following implements `srs` for ridge surfaces, seen in Fig. 1(g).

```
function vec3 fStep(vec3 x) { // ridge surfaces
    vec3{3} E = evecs( $\nabla \otimes \nabla F(x)$ );
    real{3} L = evals( $\nabla \otimes \nabla F(x)$ );
    return -(1/L{2}) * E{2} ⊗ E{2} •  $\nabla F(x)$ ;
}
function real fStrength(vec3 x) =
    evals( $\nabla \otimes \nabla F(x)$ ) {2} / (fBias + | $\nabla F(x)$ |);
```

This `fStep` and `fStrength` transcribe the mathematical definitions in (13) and (21), using the sequence (indexed by {}) of Hessian eigenvectors `E` and eigenvalues `L`. Small changes produce the ridge lines seen in Fig. 1(d).

```
function vec3 fStep(vec3 x) { // ridge lines
    vec3{3} E = evecs( $\nabla \otimes \nabla F(x)$ );
    real{3} L = evals( $\nabla \otimes \nabla F(x)$ );
    return -(E{2} ⊗ E{2} / L{2}) +
        E{1} ⊗ E{1} / L{1}) •  $\nabla F(x)$ ;
}
function real fStrength(vec3 x) =
    evals( $\nabla \otimes \nabla F(x)$ ) {1} / (fBias + | $\nabla F(x)$ |);
```

The `fStep` and `fStrength` functions for valley lines and surfaces similarly mimic their definitions in (12) and (21). Examples of `fStep` and `fStrength` functions for other extremal features (Sec. 2.2) are given with Results (Sec. 4).

3.2. Particle-based Feature Sampling

Being less common than direct volume rendering in visualization, the mechanics of particle systems and their implementation merit more detailed explanation. The Diderot program in Fig. 4 uses energy minimization to uniformly sample an isosurface. Similar to the volume renderer in Fig. 2, this uses functions `fStep`, `fPerp`, and `fStrength` (starting line 8) to isolate its specificity to isosurface features; the rest of the program is invariant with respect to the type of surface feature. The `fPerp` function returns a projection onto the space perpendicular to locally possible `fSteps`.

Based on a univariate potential energy function `phi` and its derivative (lines 14 and 15), functions `enr` and `frc` (lines 16 and 17) give the energy and force due to a particle at offset `x`, where the potential energy profile around each particle has circular support with radius `rad` (line 1). Each strand (line 19) computes the position of one particle, initialized with an initial set of points (lines 4 and 83, created by a pre-process to randomly sample the volume domain), and then updated through two stages of computation. In the first stage, while `!found` (line 29), the particle is transported onto the feature by successive applications of the `fStep` function, one step per iteration, until the step size is small enough to imply convergence, at which point `found` is set to `true` (line 35). In the second stage (line 36), each iteration computes one step of gradient descent through the potential energy created by neighboring particles (if a particle has no neighbors it creates one; line 47). This involves learning, at the current particle location `pos`, the energy and force due to neighbors (line 42), projecting out the force

```

1 input vec3 camEye ("Camera look-from point"); // look-at = [0,0,0] 26
2 input real camDepth ("Distance between near,far clip planes");
3 input real camFOV ("Vertical angle subtended by image");
4 input int imgRes ("Resolution on edge of square output image");
5 input real rayStep ("Sampling distance on central ray");
6 input real thick ("Apparent thickness of isosurface");
7 input real v0 ("which isosurface to render");
8 input image(3)[] vol ("data to render");
9 field#2(3)[] F = bspln3 @ vol; // convolve image w/ recon kernel
10 // Only these feature functions are specific to isosurfaces
11 function vec3 fStep(vec3 x) = (v0 - F(x)) * ∇F(x) / (|∇F(x)| * ∇F(x));
12 function real fStrength(vec3 x) = |∇F(x)|;
13 // Computing ray parameters and view-space basis
14 vec3 camN = normalize(-camEye); // N: away from eye
15 vec3 camU = normalize(camN × [0,0,1]); // U: right
16 vec3 camV = camN × camU; // V: down
17 real camNear = |camEye| - camDepth/2; // near clip, view space
18 real camFar = |camEye| + camDepth/2; // far clip, view space
19 // Core opacity function is a capped tent function
20 function real atent(real d) = clamp(0, 1, 1.5*(1 - |d|/thick));
21 // Renders ray through (rayU,rayV) on view plane through origin
22 strand ray(int ui, int vi) {
23     real UVmax = tan(camFOV*π/360)*|camEye|;
24     real rayU = lerp(-UVmax, UVmax, -0.5, ui, imgRes-0.5);
25     real rayV = lerp(-UVmax, UVmax, -0.5, vi, imgRes-0.5);
26
27     vec3 rayVec = camN + (rayU*camU + rayV*camV)/|camEye|;
28     real rayN = camNear - rayStep; // init ray position
29     output vec4 rgba = [0,0,0,0]; // output ray color
30     real gray = 0; // ray grayscale
31     real tt = 1; // ray transparency
32     update {
33         rayN += rayStep; // increment ray position
34         if (rayN > camFar) { // done if ray passed far plane
35             real q = 1-tt if tt < 1 else 1; // un-pre-multiply
36             rgba = [gray/q, gray/q, gray/q, 1-tt];
37             stabilize;
38         }
39         vec3 pos = camEye + rayN*rayVec; // ray sample position
40         if (!inside(pos,F) || fStrength(pos) == 0) {
41             continue; // neither in field nor possibly near feature
42         }
43         vec3 step = fStep(pos); // step towards feature
44         real aa = atent(|step|); // sample opacity
45         if (aa == 0) { continue; } // skip if no opacity
46         real gg = (normalize(step)•[0,0,1])2; // 2-sided lighting
47         gray += tt*aa*((0.2 + 0.8*gg)); // ambient and diffuse
48         tt *= 1 - aa; // transparencies multiply
49     } // end strand
50 initially [ray(ui,vi) | vi in 0..imgRes-1, ui in 0..imgRes-1];

```

Figure 2: A minimal but complete volume renderer is made specific to isosurfaces only by `fStep` and `fStrength` on lines 11 and 12.

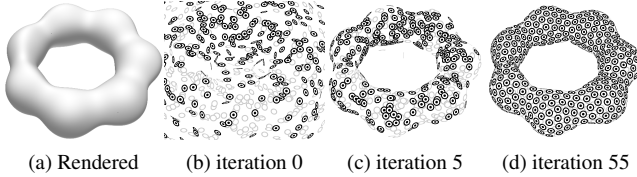


Figure 3: Minimal but complete program results: Fig. 2 volume renderer creates (a), Fig. 4 particle system creates (b), (c), and (d; converged) after indicated iterations.

component aligned with `fStep` (line 51), taking a step along force (line 52), moving back to the feature with `fStep` (line 57), and then learning the energy at the new location (line 64). The comparison of feature step length `|fs|` and energy-reducing step length `|es|` on line 58 ensures that only small steps are needed to get back to the feature, after moving to reduce energy.

Finally, line 65 tests the Armijo condition for sufficient decrease [Arm66]. In a conservative field, force is the negative gradient of potential energy, so the dot product of `-force` with the change in position (`pos - oldpos`) should predict the change in potential (`E - oldE`), which should be negative. The Armijo condition is that the actual decrease be at least some fraction of the prediction; line 65 uses fraction 0.5. If the condition is not met, the search backtracks with a smaller step size (line 66). Otherwise, the step size is slightly increased (line 70, which speeds convergence), and the number of particles in the system is adjusted. Like the individual particle motion, the determination of whether to add new particles is made locally, by each particle, based on its number of neighbors: a new particle is added if the number of neighbors is less than five (line 72). The system as a whole stabilizes (line 81) when all strands have located the feature (line 79) and no particle has undergone significant motion (line 80). Results from this program are illustrated in Fig 3b, 3c, and 3d.

The remaining particle system results below, on synthetic data here and on real-world in Sec. 4, use a more complex Diderot pro-

gram, shown in Appendix B. Its basic structure is the same as in Fig. 4, but it has three kinds of improvements: more controls on system behavior, more demanding test of system convergence, and more robust handling of population control (and the ability to sample 0D, 1D, and 2D features in 3D fields), via a an inter-particle potential function with a slight minimum. The increased system controls include the periodicity of attempts at population control (Fig. 4 does this at every iteration), a scaling of `fStep` to stabilize feature sampling, and separate convergence thresholds for feature sampling and for particle motion (Fig. 4 uses the same `eps` on lines 32 and 81).

The system convergence of the Appendix B program demands that all particles have found the feature, like the minimal particle system program above. Rather than simply requiring no significant motion in the last iteration, however, it averages motion over all recent iterations, and demands that all particles have been consistently slow-moving, and that none died or birthed new particles recently. Finally, the geometric uniformity of the sampling is directly measured with the coefficient-of-variation of each particle's distance to its closest neighbor. The coefficient-of-variation (CV) is a dimensionless measure of dispersion computed as the standard deviation divided by the mean. The particle system is uniform if all particles report a similar distance to their closest neighbor, which implies a low CV. Some of these considerations were described in earlier work on particle system [KESW09], but others (such as convergence tested with CV of distance to closest neighbor) are incremental improvements.

Better handling of particle system population (the number of particles) is required for reliable particle-based feature extraction in cases other than simple synthetic data. The system population is locally controlled according to each particle's number of neighbors, based on a minimum nn_{min} and maximum nn_{max} target number of neighbors. This permits handling 2D (surface) features, with $(nn_{min}, nn_{max}) = (6, 8)$, versus 1D (curve) features, with $(nn_{min}, nn_{max}) = (2, 3)$. To attain the target neighbor number range, particles add new neighbors with `new` (to build up the sampling of a feature that was only sparsely sampled by initialization), or remove

```

1 input real rad ("Inter-particle potential radius");
2 input real eps ("General convergence threshold");
3 input real v0 ("Which isosurface to sample");
4 input vec3[] ipos ("Initial point positions");
5 input image(3)[] vol ("Data to analyze");
6 field#2(3)[] F = bspIn3 @ clamp(vol); // convolve w/ recon kernel
7 // Only these three "f" functions are specific to isosurfaces
8 function vec3 fStep(vec3 x) = (v0 - F(x))•∇F(x)/(∇F(x)•∇F(x));
9 function tensor[3,3] fPerp(vec3 x) {
10    vec3 norm = normalize(∇F(x));
11    return identity[3] - norm⊗norm;
12 }
13 function real fStrength(vec3 x) = |∇F(x)|;
14 function real phi(real r) = (1 - r)^4; // univariate potential
15 function real phi'(real r) = -4*(1 - r)^3;
16 function real enr(vec3 x) = phi(|x|/rad);
17 function vec3 frc(vec3 x) = phi'(|x|/rad) * (1/rad) * x/|x|;
18 // Strands first find feature, then interact w/ or make neighbors
19 strand point (vec3 pos0, real hh0) {
20    output vec3 pos = pos0; // current particle position
21    real hh = hh0; // energy gradient descent stepsize
22    vec3 step = [0,0,0]; // energy+feature steps this iter
23    bool found = false; // whether feature has been found
24    int nfs = 0; // number feature steps taken
25    update {
26        if (!inside(pos, F) || fStrength(pos) == 0) {
27            die; // not in field domain & not possibly near feature
28        }
29        if (!found) { // looking for feature
30            step = fStep(pos); // one step towards feature
31            pos += step;
32            if (|step|/rad > eps) { // took a substantial step
33                nfs += 1;
34                if (nfs > 10) { die; } // too slow to converge
35            } else { found = true; } // else converged on feature
36        } else { // feature found; interact with other points
37            pos += fStep(pos); // refine feature sampling
38            step = [0,0,0]; // initialize output step
39            real oldE = 0; // energy at current location
40            vec3 force = [0,0,0]; // force on me from neighbors
41            int nn = 0; // number of neighbors
42            foreach (point P in sphere(rad)) {
43                oldE += enr(P.pos - pos);
44                force += frc(P.pos - pos);
45                nn += 1;
46            }
47            if (0 == nn) { // no neighbors, so create one
48                new point(pos + [0.5*rad,0,0], hh);
49                continue;
50            }
51            force = fPerp(pos)•force; // no force perp. to fStep(pos)
52            vec3 es = hh*force; // energy step along force
53            if (|es| > rad) { // limit motion to radius
54                hh *= rad/|es|; // decrease stepsize and step
55                es *= rad/|es|;
56            }
57            if (|fs|/|es| > 0.5) { // feature step too big
58                hh *= 0.5; // try again w/ smaller step
59                continue;
60            }
61            vec3 fs = fStep(pos+es); // find step towards feature
62            if (|fs|/|es| > 0.5) { // feature step too big
63                hh *= 0.5; // try again w/ smaller step
64                continue;
65            }
66            pos += fs + es; // take steps, find new energy
67            real newE = sum { enr(pos - P.pos) | P in sphere(rad) };
68            if (newE - oldE > 0.5*(pos - oldpos)•(-force)) {
69                pos = oldpos; // energy didn't go down enough;
70                hh *= 0.5; // try again w/ smaller step
71                continue;
72            }
73            hh *= 1.1; // cautiously increase stepsize
74            step = fs + es; // record steps taken
75            if (nn < 5) { // add neighbor if have too few
76                new point(pos + 0.5*rad*normalize(es), hh);
77            }
78        } // else found
79    } // update
80    global {
81        bool allfound = all { P.found | P in point.all};
82        real maxstep = max { |P.step| | P in point.all };
83        if (allfound && maxstep/rad < eps) { stabilize; }
84    }
85 initially { point(ipos[ii], 1) | ii in 0 .. length(ipos)-1 };

```

Figure 4: A minimal but complete surface feature sampler is made specific to isosurfaces only by three feature functions starting line 8.

themselves with **die** (to remove points from needlessly dense samplings). Particles next to the boundary of a feature, where feature strength falls below a threshold, will be missing some neighbors, and will thus try to create new neighbors. These new particles will be immediately removed, however, because of **featureOut** (as with line 26 of Fig. 4) To prevent a continuous stream of short-lived particles dying at feature boundaries, each particle maintains a count of how many new neighbors it has created, which is capped at nn_{max} .

A final conceptual difference between the simplistic particle program in Fig. 4 and the robust one in Appendix B is the sampling of features with boundaries. While inter-particle repulsion is adequate for most isosurfaces (as seen in Figure), problems arise when the isosurface is not entirely contained by the volume domain, or when the feature is not a closed surface, as with the open edge of a ridge surface where the feature strength falls below a threshold. In these cases, simple repulsion will force particles off the feature, failing to maintain a regular hexagonal sampling on surface features. Following previous work [KESW09], we create a radial potential function $\phi(r)$ with a slight potential well (with negative energy) to create a specific preferred distance between particles. Current work has adopted the $\phi(r)$ shown in (Appendix B) Fig. 9, a C^3 -continuous function from $\phi(0) = 1$ to $\phi(r) = 0$ for $r \geq 1$, with a minima (well) at $\phi(2/3) = -0.001$.

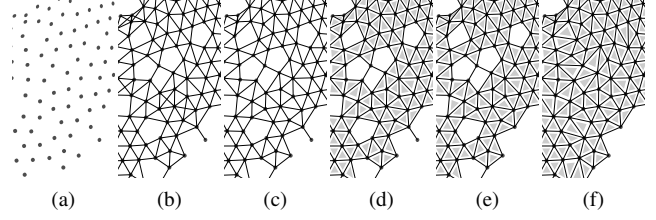


Figure 5: Particles on surface features (a) are post-processed to make meshes: edges for all inter-particle contacts (b), uncrossing edges (c), triangles (d), and fixing edges (e) and holes (f).

3.3. Particle system post-processing

After computing a particle system to sample a surface feature, meshing the resulting points may be more useful for down-stream processing or visualization than the point locations themselves. We believe the high spatial regularity at convergence of our particle systems, combined with erring on the side of high sampling density, simplifies the meshing task. Our simple meshing approach has proven adequate for results so far, though it would benefit from careful computational geometry analysis. Fig 5 illustrates the approach for an intermediate (non-converged) configuration with less regularity (Fig 5a). We first find edges for all inter-particle interactions (i.e. within each other's potential wells, Fig 5b), using a short utility Diderot program described in Appendix D.2. Subsequent steps are implemented in about 700 lines of C code. We then find crossing edge pairs, and remove the longer edge in each

pair (Fig 5c). We add triangles for length-3 edge loops (Fig 5d), and remove stray edges (Fig 5e). Short edge loops (length 4 or 5) with only one triangle per edge are holes, which we fill by adding minimal-length internal edges and associated triangles. This approach produced the meshes seen in the lower row of Fig 1. To connect particle samplings of 1D features into polylines, we simply add edges for inter-particle interactions.

4. Results

These results were produced with the volume rendering and particle system programs in Appendices A and B, modified for each case by defining the field F of interest, and selecting the feature functions for the feature type of interest. The code for the feature functions are shared between the two programs.

4.1. Cell Nuclei as Local Maxima

Microscopic volumetric imaging often involves manipulating specimen so that cell nuclei fluoresce [Str07], so that maximum intensity projection (MIP) can visualize the location of nuclei [LZP12]. Fig. 6a illustrates an example of this, in an setting where a cell sub-

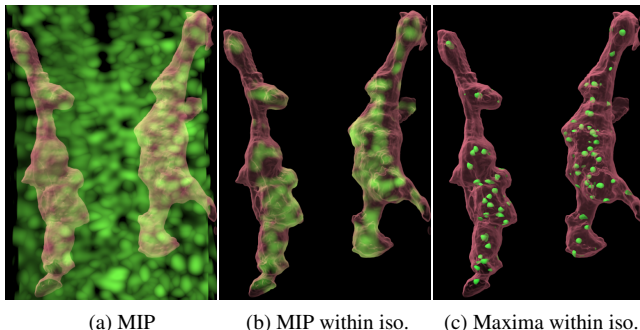


Figure 6: Green cell nuclei can be traditionally rendered with MIP (a), or with MIP computed only within the membrane of cells of interest (b). Maxima rendering (c) clarifies nuclei number and depth.

population of particular interest exhibits red fluorescence in their cell membrane (seen as an isosurface), in addition to the nuclei in green. In Fig. 6b, the MIP is computed only within the interior of the cells of interest, which clarifies the result somewhat by removing the contribution of the nuclei from other cells. The individual nuclei remain hard to discern, however. Fig. 6c renders the *local maxima only*, using the critical point step function (8), so that the number, location, and relative position of the nuclei become clear, as each is rendered as a shaded and roughly spherical blob. This is not possible with isosurface rendering: the local maxima for each nuclei occur at widely varying intensities, so isosurfacing could not consistently reveal them all, nor create a spherical shape from maxima with different (negative) Hessian eigenvalues.

4.2. Ridge Surface Boundary Curve

While it is common in practice to bound the extent of ridge surface features by thresholding their feature strength, they also

have an intrinsic boundary at certain degeneracies of the Hessian, where its two smallest eigenvalues become equal, as described by Schultz et al. [STS10]. They localize degeneracies on voxel faces with Newton steps towards the simultaneous roots of a set of discriminant functions of the Hessian components [ZP04], and then connect a polyline of degenerate Hessians across faces. Our approach starts by defining a new scalar field as the *mode* of the Hessian [CHDH00] (which is +1 when its two smaller eigenvalues are equal, and -1 when its two larger eigenvalues are equal). We copy formulae from [CHDH00] to create a scalar field F of Hessian mode:

```
field#4[] F0 = c4hexic ⊗ img; // img == data volume
field#2(3)[3,3] E = ∇⊗∇F0 - identity[3]*trace(∇⊗∇F0)/3;
field#2(3)[] F = 3*sqrt(6)*det(E/|E|);
```

Then ridge lines of mode F , where it is close to 1, are the degenerate lines of interest. Fig 7 illustrates with a synthetic dataset in-

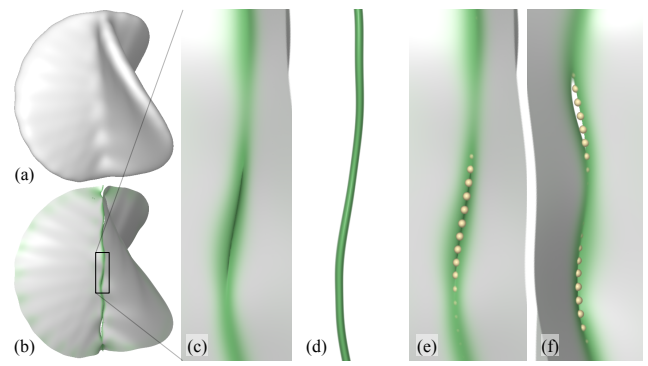


Figure 7: A three-way intersection of sheets (a) creates a complex configuration of ridge surfaces (b), seen closer in (c). The analytic ridge boundary can be rendered in isolation (d), and regularly sampled with a particle system (e); different view (f).

volving three twisting sheets meeting in the middle. The resolution and orientation of the volume sampling grid combined with the reconstruction gives rise to a particular configuration of two sheets joining, and one terminating at a degenerate line. We may now easily volume render the degenerate line in isolation as a ridge line of mode (Fig 7d), or explicitly sample it with a particle system, and then render the particles in the context of the original volume (Fig 7e,f). The feature step fStep function used to render or sample the degenerate line is the same as for ridge lines in Sec. 3.1; only the definition (above) of scalar field F differs. While the previous Newton-step approach for isolating these features use trilinear interpolation of third derivatives [STS10,ZP04], ours requires fourth derivatives (Hessian of the mode of the Hessian), but with significantly smaller implementation complexity, and the ability to work with high-quality reconstructions.

4.3. Crease Lines on Implicit Surfaces

While volume rendering transfer functions based on curvature can highlight the convex and concave portions of implicit surfaces [HKG00,KWTF03], Fig 8a illustrates that they do a poor job of capturing surface creases (Sec 2.2) on a synthetic volume of a dodecahedron with indented faces and edges of varying sharpness. To render crease lines properly, we create a scalar

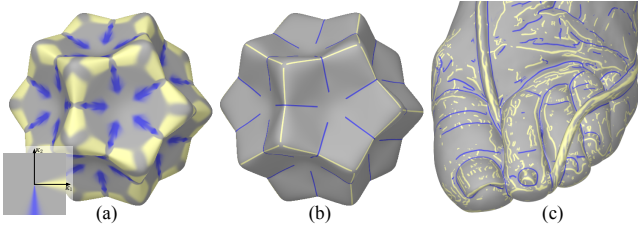


Figure 8: Curvature-based transfer functions do a poor job (a) of isolating surface crease lines, but feature steps toward curvature extrema permit their clean rendering (b), (c).

fields K_1 and K_2 of curvature, based on formulae in [KWTM03]:

```
field#3(3)[3] N = - $\nabla F$  / | $\nabla F$ |; //  $F=C^4$  scalar field
field#3(3)[3,3] P = identity[3] - N $\otimes$ N; // evals=1,1,0
field#2(3)[3,3] G = P $\bullet$ ( $\nabla \otimes N$ )P; // evals=k1,k2,0
field#2(3)[] discrim = sqrt(2*G:G - trace(G) $\star$ trace(G));
field#2(3)[] K1 = (trace(G) + discrim)/2;
field#2(3)[] K2 = (trace(G) - discrim)/2;
field#2(3)[] KT = sqrt(K1 $\wedge$  K2 $\wedge$ );
```

Rendering crease lines does not require creating a new function to $fStep$ in 3D towards the curvature extrema, but we do require the length of that step. Outward creases (maxima of K_1 along d_1) are rendered by setting material color $mcol$ via:

```
1 if (KT(pos) < fMaskTh) {
2     mcol = gray; // low total curvature, uninteresting
3 } else {
4     vec3 d1 = colspans(G(pos) - K2(pos) * P(pos));
5     real k1' = d1 $\bullet$ VK1(pos);
6     real k1'' = d1 $\bullet$ ( $\nabla \otimes \nabla K_1$ (pos)) $\bullet$ d1;
7     mcol = lerp(gray, rcol, atent(1, |k1'/k1''|/3));
8 }
```

where $gray$ and $rcol$ are the colors for gray and the outward crease color; the code for inward crease rendering is essentially the same. The tensor $G(pos) - K2(pos) * P(pos)$ on line 4 has eigenvalues $k_1, 0, 0$; utility function $colspans$ (App. D.1) returns the eigenvector (i.e. the curvature direction d_1) for k_1 . From (15), the crease line feature step length is $|k1'/k1''|$, used on line 7 with the same $atent$ of Fig. 2 line 20 to effect the crease line coloring, shown in Fig. 8b. Results on a foot of the Visible Human female CT scan are in Fig. 8c. The registration cord, with its nearly constant curvature, represents a particular challenge, but other creases clearly indicate skin folds and toenail edges, while the valleys demarcate the toenails, the toes themselves, and the edge of the registration cord. The ease of creating these renderings, which depend on fourth derivatives (Hessian of curvature), is notable.

4.4. Vortex Cores in 3D Flow

... Sujadi/Haimes vortex cores

Our work on Parallel Vector Operator features also includes potentially novel formulae for the gradient and Hessian of the dot product $(\mathbf{a}/|\mathbf{a}|) \cdot (\mathbf{b}/|\mathbf{b}|)$ between two vector fields \mathbf{a} and \mathbf{b} , normalized. For Sujadi-Haimes vortex cores of vector field \mathbf{v} , $\mathbf{a} = \mathbf{v}$ and $\mathbf{b} = (\nabla \otimes \mathbf{v})\mathbf{v}$. We were able to modify the open-source Diderot compiler to expose some of its intermediate representation to reveal the expressions it used to compute the vector flow results above. The results, and a comparison with formulae from the PVsolve solve method of Van Gelder and Pang [GP09], are described in Appendix C.

4.5. Anisotropy Extremal Surfaces

... extrema of anisotropy WRT DTI tensor eigenvectors

5. Related Work

Barakat et al. introduced different methods to render [BT10] and extract [BAT11] crease surfaces separately, while our method bridges the gap between volume rendering and surface extraction by the means of a single step function. The underlying techniques proposed by Barakat et al. are also fundamentally different from our approach. In [BT10], the authors focus on an interactive approach to rendering crease surfaces, which utilizes multiple space skipping strategies and iterative search for finding crease features. The rendering is sensitive to various parameters that users need to control on the fly. In contrast, our rendering method does not need to find the exact sample along the surface but relies on a single Newton-Raphson step approximation with less dependencies on user input. In [BAT11], an advancing front approach is proposed to extract crease surfaces, which iteratively samples new points and grows the triangular mesh based on an estimated error to the crease surface. On the other hand, our method first uniformly samples feature points along the surface, then builds the triangular mesh by cleverly connecting the obtained points. The uniform nature of the sampled points provides a fairly regular triangular mesh compared to that of [BAT11].

... [KCS*16] demonstrated volume rendering of fuzzy isocontours (using a Levoy opacity function) of scalar quantities derived from scalar, vector, and tensor fields, and described a particle system for uniformly sampling isocontours of scalar fields. Our current work is focused on the more general extremal features.

Knoll et al. [KHW*09] introduced a method to find locations corresponding to the peaks in 1D transfer function in order to perform sampling at these peaks. Kotava et al. [KKS*12] extended this approach to multidimensional transfer functions. Although these methods are similar to ours with respect to the interest of peaks and extrema, the context and underlying principles are fundamentally different. While their effort is to find peaks in transfer function domain to provide location for enhanced sampling, we are interested in a general approach to finding the extrema in scalar field for visualizing and extracting features of interest. Our method provides Newton-Raphson based analytical one-step approximation of the distance from a point to its local extrema, which is directly utilized to provide novel means for visualization, in contrast to pre-integration and secant based method of iteratively finding peaks in [KHW*09].

Relative to earlier work with Diderot, we advance generality with respect to feature type, the combination of visualization and extraction of a range of extremal features (instead of only isosurfaces), and much more sophisticated particle-based feature extraction (with meshing, in 3-D, instead of only 2-D sampling).

6. Discussion, Conclusions, Future Work

Our new approach unifies, both in mathematical formulation and in source code, the tasks of volume rendering and geometrically

extracting features of interest in 3D fields. These are complementary tasks: one can quickly volume render to ascertain the presence of features, and set appropriate feature strength and feature mask (Sec. 2.3) thresholds, before running feature extraction and meshing. Any regions of problematic feature extraction can be inspected and diagnosed by high quality rendering that directly visualizes the underlying field and the mathematical ingredients of its features. Being able to use the same code to describe features for both tasks increases trust in the results, and being able to write code that mirrors traditional math notation simplifies how users may translate new research ideas to working code. Our work may also rekindle interest in existing features, like surface creases (Sec. 2.2 and Fig. 8), by dramatically decreasing the required code complexity.

The focus of this work has been establishing the viability of a new way of implementing scientific visualization research, to address the bottleneck of human implementation time, rather than computational execution time. Still, the volume rendering and particle system programs can both execute in parallel, which makes them workable with sufficient cores, but we did record any specific measurements of compile time, execution time, or parallel speedup. On a modern Mac laptop with 8 cores, most programs compiled in under 20 seconds, though particle systems on vector and tensor data took up to 2 minutes. Execution times ranged from under 5 seconds for scalar volume renderings, to several minutes for the more complex particle systems. One drawback to Diderot for our approach is that any change to the field or feature functions requires recompiling the entire program. We would like to explore compiling feature functions into modules that may be dynamically linked into a pre-compiled Diderot executable, but this is complicated by the whole-program optimization currently performed by the Diderot compiler.

Though the volume rendering and feature sampling programs are mature enough to work on real data, they favor implementation simplicity over computational efficiency or algorithmic sophistication. We would like to explore adaptive sampling of rays and along rays in volume rendering, so that less effort is spent on samples contributing zero opacity, allowing higher-quality renderings for the same cost. It may be possible to generalize the Lipschitz constants used by Kalra and Barr for implicit surface ray casting to other features [KB89]. The current particle system approach makes no effort to vary particle density with feature curvature [MGW05], or discover the best scale at which to find features [KESW09]. Nor does it have the ability to first sample the elements of a feature complex in order of decreasing codimension (e.g. critical points, then connecting curves, then separating surfaces) [MWK*08]. Implementing these more advanced techniques is hampered somewhat by the absence of a Diderot debugger.

Except for the C code for particle system meshing (Sec. 3.3), all the code for generating our results is in Diderot, and all of it is included in this manuscript and its Appendices. While mature visualization applications will likely require connections to other libraries and interfaces, we are holding ourselves to a standard for self-contained reproducibility that we believe may cultivate research interest in scientific visualization by simplifying how readers may explore and experiment with new methods.

References

- [AK04] AMENTA N., KIL Y. J.: Defining point-set surfaces. In *Computer Graphics (Proc. ACM SIGGRAPH) 2004* (2004), pp. 264–270. 2, 3
- [Arm66] ARMIJO L.: Minimization of functions having Lipschitz continuous first partial derivatives. *Pac. J. Math.* 16, 1 (1966), 1–3. 6
- [BAT11] BARAKAT S., ANDRYSCO N., TRICOCHE X.: Fast extraction of high-quality crease surfaces for visual analysis. *Computer Graphics Forum* 30, 3 (2011), 961–970. [doi:10.1111/j.1467-8659.2011.01945.x](https://doi.org/10.1111/j.1467-8659.2011.01945.x). 9
- [BT10] BARAKAT S., TRICOCHE X.: An image-based approach to interactive crease extraction and rendering. *Procedia Computer Science* 1, 1 (2010), 1709 – 1718. ICCS 2010. [doi:https://doi.org/10.1016/j.procs.2010.04.192](https://doi.org/10.1016/j.procs.2010.04.192). 9
- [CA97] CROSSNO P., ANGEL E.: Isosurface extraction using particle systems. In *Proc. IEEE Visualization* (1997), pp. 495–498. 3
- [Car76] CARMO M. D.: *Differential Geometry of Curves and Surfaces*. Prentice-Hall, Inc., Englewood Cliffs, New Jersey, 1976. 4
- [CHDH00] CRISCIONE J. C., HUMPHREY J. D., DOUGLAS A. S., HUNTER W. C.: An invariant basis for natural strain which yields orthogonal stress response terms in isotropic hyperelasticity. *Journal of Mechanics and Physics of Solids* 48 (2000), 2445–2465. 8
- [Chi17] CHIW C.: *Implementing mathematical expressiveness in Diderot*. PhD thesis, University of Chicago, Chicago, IL, May 2017. 2, 4
- [CHJ03] CO C. S., HAMANN B., JOY K. I.: Iso-splatting: a point-based alternative to isosurface visualization. In *Proc. 11th Pacific Conference on Computer Graphics and Applications* (Oct. 2003), pp. 325–334. [doi:10.1109/PCCGA.2003.1238274](https://doi.org/10.1109/PCCGA.2003.1238274). 3
- [CKR*12] CHIW C., KINDELMANN G., REPPY J., SAMUELS L., SELTZER N.: Diderot: A Parallel DSL for image analysis and visualization. In *Proc. SIGPLAN 2012 Conference on Programming Language Design and Implementation (PLDI)* (June 2012), pp. 111–120. 2, 4
- [Ebe96] EBERLY D.: *Ridges in Image and Data Analysis*. Kluwer Academic Publishers, 1996. 2, 3
- [GM97] GUY G., MEDIONI G.: Inference of surfaces, 3d curves, and junctions from sparse, noisy, 3d data. *IEEE Transactions on Pattern Analysis and Machine Intelligence* 19, 11 (Nov 1997), 1265–1277. [doi:10.1109/34.632985](https://doi.org/10.1109/34.632985). 3
- [GP09] GELDER A. V., PANG A.: Using PVsolve to analyze and locate positions of parallel vectors. *IEEE Transactions on Visualization and Computer Graphics* 15, 4 (July 2009), 682–695. [doi:10.1109/TVCG.2009.11](https://doi.org/10.1109/TVCG.2009.11). 9, 16
- [Har83] HARALICK R. M.: Ridges and valleys on digital images. *Computer Vision, Graphics, and Image Processing* 22 (1983), 28–38. 2, 4
- [HKG00] HLADUVKA J., KÖNIG A., GRÖLLERRÖLLER E.: Curvature-based transfer functions for direct volume rendering. In *Spring Conference on Computer Graphics 2000* (May 2000), vol. 16, pp. 58–65. 9
- [KB89] KALRA D., BARR A. H.: Guaranteed ray intersections with implicit surfaces. In *Computer Graphics (Proc. ACM SIGGRAPH) 1989* (1989), pp. 297–306. 10
- [KCS*16] KINDELMANN G., CHIW C., SELTZER N., SAMUELS L., REPPY J.: Diderot: a domain-specific language for portable parallel scientific visualization and image analysis. *IEEE Trans. on Visualization and Computer Graphics (Proceedings VIS 2015)* 22, 1 (Jan. 2016), 867–876. [doi:10.1109/TVCG.2015.2467449](https://doi.org/10.1109/TVCG.2015.2467449). 2, 4, 9
- [KESW09] KINDELMANN G. L., ESTÉPAR R. S. J., SMITH S. M., WESTIN C.-F.: Sampling and visualizing creases with scale-space particles. *IEEE Trans. on Visualization and Computer Graphics* 15, 6 (2009), 1415–1424. 6, 7, 10
- [KHW*09] KNOLL A., HIJAZI Y., WESTERTEIGER R., SCHOTT M., HANSEN C., HAGEN H.: Volume ray casting with peak finding and differential sampling. *IEEE Transactions on Visualization and Computer*

- Graphics* 15, 6 (2009), 1571–1578. doi:10.1109/TVCG.2009.204. 9
- [KKS*12] KOTAVA N., KNOLL A., SCHOTT M., GARTH C., TRICOCHE X., KESSLER C., COHEN E., HANSEN C. D., PAPKA M. E., HAGEN H.: Volume rendering with multidimensional peak finding. *IEEE Pacific Visualization Symposium 2012, PacificVis 2012 - Proceedings vi* (2012), 161–168. doi:10.1109/PacificVis.2012.6183587. 9
- [Koe90] KOENDERINK J. J.: *Solid Shape*. The MIT Press, 1990. 4
- [KWTM03] KINDLMANN G., WHITAKER R., TASDIZEN T., MÖLLER T.: Curvature-based transfer functions for direct volume rendering: Methods and applications. In *Proc. IEEE Visualization 2003* (2003), pp. 513–520. 9
- [LC87] LORENSEN W. E., CLINE H. E.: Marching cubes: A high resolution 3D surface construction algorithm. *Computer Graphics* 21, 4 (1987), 163–169. 2
- [Lev88] LEVOY M.: Display of surfaces from volume data. *IEEE Computer Graphics & Applications* 8, 5 (1988), 29–37. 2
- [LHRS05] LEVET F., HADIM J., REUTER P., SCHLICK C.: Anisotropic sampling for differential point rendering of implicit surfaces. In *Proc. 13th Intl. Conf. in Central Europe on Computer Graphics, Visualization, and Computer Vision, WSCG 2005* (2005), pp. 109–116. 3
- [LZP12] LONG F., ZHOU J., PENG H.: Visualization and Analysis of 3D Microscopic Images. *PLoS Computational Biology* (2012). 8
- [MB95] MONGA O., BENAYOUN S.: Using partial derivatives of 3D images to extract typical surface features. *Computer Vision and Image Understanding* 61, 2 (March 1995), 171–189. 4
- [MGW05] MEYER M. D., GEORGEL P., WHITAKER R. T.: Robust particle systems for curvature dependent sampling of implicit surfaces. In *Proc. Shape Modeling and Applications (SMI)* (June 2005), pp. 124–133. 3, 10
- [MLD94] MONGA O., LENGAGNE R., DERICHE R.: Crest lines extraction in volume 3d medical images: a multi-scale approach. In *Proceedings of 12th International Conference on Pattern Recognition* (Oct 1994), vol. 1, pp. 553–555 vol.1. doi:10.1109/ICPR.1994.576356. 4
- [MWK*08] MEYER M., WHITAKER R., KIRBY R. M., LEDERGERBER C., PFISTER H.: Particle-based sampling and meshing of surfaces in multimaterial volumes. *IEEE Trans. on Visualization and Computer Graphics* 14, 6 (Nov–Dec 2008), 1539–1546. 10
- [NKH13] NELSON B., KIRBY R. M., HAIMES R.: Gpu-based volume visualization from high-order finite element fields. *IEEE Transactions on Visualization & Computer Graphics* 20, 1 (2013), 70–83. doi:10.1109/TVCG.2013.96. 2
- [NLKH12] NELSON B., LIU E., KIRBY R. M., HAIMES R.: Elvis: A system for the accurate and interactive visualization of high-order finite element solutions. *IEEE Transactions on Visualization and Computer Graphics* 18, 12 (Dec. 2012), 2325–2334. doi:10.1109/TVCG.2012.218. 2
- [OMD*12] OBERMAIER H., MOHRING J., DEINES E., HERING-BERTRAM M., HAGEN H.: On mesh-free valley surface extraction with application to low frequency sound simulation. *Visualization and Computer Graphics, IEEE Transactions on* 18, 2 (2012), 270–282. 3
- [PR99] PEIKERT R., ROTH M.: The "parallel vectors" operator - a vector field visualization primitive. In *Proc. IEEE Visualization* (1999), pp. 263–270. 2, 16
- [PS08] PEIKERT R., SADLO F.: Height ridge computation and filtering for visualization. In *Proc. Pacific Vis* (March 2008), Fujishiro I., Li H., Ma K.-L., (Eds.), pp. 119–126. 2
- [SH94] SUJUDI D., HAIMES R.: *Identification of Swirling Flow in 3D Vector Fields*. Tech. rep., Dept. of Aeronautics and Astronautics, MIT, Cambridge, MA, 1994. 4
- [SP07] SADLO F., PEIKERT R.: Efficient visualization of lagrangian coherent structures by filtered AMR ridge extraction. *IEEE Trans. on Visualization and Computer Graphics (Proc. Visualization)* 13, 6 (Nov 2007), 1456–1463. 2
- [Str07] STRAIGHT A. F.: Fluorescent protein applications in microscopy. In *Digital Microscopy, 3rd Edition*, vol. 81 Supplement C of *Methods in Cell Biology*. Academic Press, 2007, pp. 93 – 113. doi:10.1016/S0091-679X(06)81006-X. 8
- [STS10] SCHULTZ T., THEISEL H., SEIDEL H.-P.: Crease surfaces: From theory to extraction and application to diffusion tensor MRI. *IEEE Trans. on Visualization and Computer Graphics* 16, 1 (2010), 109–119. 3, 4, 8
- [SWTH07] SAHNER J., WEINKAUF T., TEUBER N., HEGE H. C.: Vortex and strain skeletons in eulerian and lagrangian frames. *IEEE Transactions on Visualization and Computer Graphics* 13, 5 (Sept. 2007), 980–990. doi:10.1109/TVCG.2007.1053. 3
- [TKW08] TRICOCHE X., KINDLMANN G., WESTIN C.-F.: Invariant crease lines for topological and structural analysis of tensor fields. *IEEE Trans. on Visualization and Computer Graphics* 14, 6 (2008), 1627–1634. 2
- [TM98] TANG C.-K., MEDIONI G.: Extremal feature extraction from 3-D vector and noisy scalar fields. In *Proc. IEEE Visualization '98* (Oct. 1998), pp. 95–102. 2, 3
- [WH94] WITKIN A. P., HECKBERT P. S.: Using particles to sample and control implicit surfaces. *Computer Graphics (Proc. ACM SIGGRAPH)* 28 (1994), 269–277. 3
- [ZP04] ZHENG X., PANG A.: Topological lines in 3d tensor fields. In *Proc. IEEE Visualization 2004* (Oct. 2004), pp. 313–320. doi:10.1109/VISUAL.2004.105. 8
- [ZS17] ZOBEL V., SCHEUERMANN G.: Extremal curves and surfaces in symmetric tensor fields. *The Visual Computer* (Oct. 2017). doi:10.1007/s00371-017-1450-1. 3

Appendix A: Direct Volume Rendering in Diderot

The base program for the direct volume rendered figures is below. It was used as-is for Fig. 1. The program comments should support understanding its operation; some additional explanation follows.

```

1  input vec3 camEye ("camera look-from point");
2  input vec3 camAt ("camera look-at point");
3  input vec3 camUp ("camera pseudo-up vector");
4  input real camNear ("at-relative near clip distance");
5  input real camFar ("at-relative far clip distance");
6  input real camFOV ("vertical field-of-view angle");
7  input bool camOrtho ("orthographic (not perspective)") = false;
8  input int iresU ("image # horizontal samples");
9  input int iresV ("image # vertical samples");
10 input real rayStep ("ray inter-sample distance");
11 input real refStep ("opacity reference step length");
12 input real transp0 ("early ray stopping transparency") = 0.005;
13 input real thick ("approximate thickness of feature");
14 input real fStrTh ("feature strength threshold");
15 input real fMaskTh ("feature mask threshold") = 0;
16 input real fBias ("Bias in feature strength computing") = 0.0;
17 input real maxAlpha ("maximum opacity of feature");
18 input vec4 phong ("Phong Ka Kd Ks Sp") = [0.1, 0.7, 0.2, 100];
19 input vec3 litdir ("view-space light direction") = [-1,-2,-1];
20 input vec3 mcNear ("color at near clip plane") = [1,1,1];
21 input vec3 mcFar ("color at far clipping plane") = [1,1,1];
22 input real isoval ("which isosurface to render");
23 input image(3)[] vol ("data to render") = image("vol.nrrd");
24 input image(1)[3] cmap ("scalar colormap") = image("cmap.nrrd");
25 input vec2 cmmm ("min,max colormap range") = [0,0];
26
27 field#2(3)[] F = bspln3 ⊗ clamp(vol);
28 field#0(3)[] Fcm = F; // colormap scalar field itself
29 field#0(1)[3] CM = tent ⊗ clamp(cmap); // 1-D colormap field
30
31 // Isosurface-specificity limited to these four functions
32 function vec3 fStep(vec3 x) =
33 | (isoval - F(x)) * ∇F(x) / (∇F(x) • ∇F(x));
34 function real fStrength(vec3 x) = |∇F(x)|;
35 function real fMask(vec3 x) = F(x);
36 function bool fTest(vec3 x) = true;
37
38 // Computing ray parameters and view-space basis
39 vec3 camN = normalize(camAt - camEye); // N: away from eye
40 vec3 camU = normalize(camN × camUp); // U: right
41 vec3 camV = camN × camU; // V: down
42 real camDist = |camAt - camEye|;
43 real camMax = tan(camFOV * π / 360) * camDist;
44 real camUmax = camVmax * iresU / iresV;
45 real camNearVsp = camNear + camDist; // near clip, view space
46 real camFarVsp = camFar + camDist; // far clip, view space
47
48 // Convert light direction from view-space to world-space
49 vec3 litwsp = transpose([camU, camV, camN]) • normalize(litdir);
50
51 // Core opacity function is a capped tent function
52 function real atent(real a0, real d)
53 | = a0 * clamp(0, 1, 1.5 * (1 - |d| / thick));
54
55 function bool postTest(vec3 x)
56 | = (inside(x, F) // in field
57 && fStrength(x) > fStrTh // possibly near feature
58 && fMask(x) >= fMaskTh // meets feature mask
59 && fTest(x)); // passes addtl feature criterion
60
61 // Each strand renders one ray through (rayU,rayV) on view plane
62 strand raycast(int ui, int vi) {
63 // Compute geometry of ray through pixel [ui,vi]
64 real rayU = lerp(-camUmax, camUmax, -0.5, ui, iresU - 0.5);
65 real rayV = lerp(-camVmax, camVmax, -0.5, vi, iresV - 0.5);
66 real rayN = camNearVsp;
67 vec3 UV = rayU * camU + rayV * camV;
68 vec3 rayOrig = camEye + (UV if camOrtho else [0,0,0]);
69 vec3 rayVec = camN + ([0,0,0] if camOrtho else UV / camDist);
70
71 // Opacity correction is via alphaFix; distance between
72 // ray samples is |rayVec| * rayStep
73 real alphaFix = |rayVec| * rayStep / refStep;
74 vec3 eyeDir = -normalize(rayVec);
75
76 // Unpack Phong parameters
77 real phKa = phong[0]; real phKd = phong[1];
78 real phKs = phong[2]; real phSp = phong[3];
79
80 output vec4 rgba = [0,0,0,0]; // ray output
81 vec3 rgb = [0,0,0]; // ray state is current color ...
82 real transp = 1; // ... and current transparency
83

```

```

84 update {
85     rayN += rayStep;           // increment ray position
86     if (rayN > camFarVsp) {   // ray passed far clip plane
87         stabilize;
88     }
89     vec3 pos = rayOrig + rayN*rayVec; // ray sample position
90     if (!posTest(pos)) {
91         continue;
92     }
93
94     vec3 step = fStep(pos);      // step towards feature
95     real aa = atent(maxAlpha, |step|); // opacity
96     if (aa == 0) { continue; }    // skip if no opacity
97     aa = 1 - (1 - aa)^alphaFix; // opacity correction
98     vec3 snorm = -normalize(step); // "surface normal"
99     real dcomp = (snorm*litwsp)^2; // two-sided lighting
100    real scomp = |snorm|normalize(eyeDir+litwsp)|^phSp
101        if phKs != 0 else 0.0;
102
103    // simple depth-cueing
104    vec3 dcol = lerp(mcNear, mcFar, camNearVsp, rayN, camFarVsp);
105    vec3 mcol = CM(lerp(0, 1, cmmm[0], Fcm(pos+step), cmmm[1]));
106        if (cmmm[0] != cmmm[1]) else [1,1,1];
107    // light color is [1,1,1]
108    rgb += transp*aa*(phKa + phKd*dcomp)*modulate(dcol,mcol)
109        + phKs*scomp*[1,1,1]);
110    transp *= 1 - aa;
111    if (transp < transp0) { // early ray termination
112        transp = 0;
113        stabilize;
114    }
115}
116 stabilize {
117     if (transp < 1) { // un-pre-multiply opacities
118         real aa = 1-transp;
119         rgba = [rgb[0]/aa, rgb[1]/aa, rgb[2]/aa, aa];
120     }
121 }
122 }
123 initially [ raycast(ui, vi)
124             | vi in 0..iresV-1, ui in 0..iresU-1 ];

```

The renderer is made specific to isosurface with the feature step `fStep` (line 32) and feature strength `fStrength` (line 34) functions. As described in Sec. 2 and demonstrated in Secs. 3 and 4, different feature step and strength functions will repurpose the renderer for different types of features. Vector and tensor field rendering will involve defining some derived scalar field `F` from the multi-variate data, rather than directly creating `F` from the data as in line 27 above. The feature mask function `fMask` (line 35) was described in Sec. 2.3 additional tunable control over what parts of a feature are worth seeing, and the test function `fTest` (line 36) is available as a further criterion for feature membership. These are used in the `postTest` function (line 55) function, which used on line 90 to skip over some ray samples.

Appendix B: Particle-based Feature Sampling in Diderot

The base program for the particle-based feature sampling is below. It was used as-is for Fig. 1f. The program comments should support understanding its operation; additional explanations follow.

```

1  input real fStrTh ("Feature strength threshold");
2  input real fMaskTh ("feature mask threshold") = 0;
3  input real fbias ("Bias in feature strength computing") = 0.0;
4  input real tipd ("Target inter-particle distance");
5  /* tipd is the only length or speed variable with data spatial
   units; everything else measures space in units of tipd */
6
7  input real mabd ("Min allowed birth distance (> 0.7351)") = 0.75;
8  input real travMax ("Max allowed travel to or on feature") = 10;
9  input int nfsMax ("Max allowed # feature steps") = 20;
10 // these next three control the Gradient Descent in Energy
11 input real gdeTest ("Scaling in sufficient decrease test") = 0.5;
12 input real gdeBack ("How to scale stepsize for backtrack") = 0.5;
13 input real gdeOppor ("Opportunistic stepsize increase") = 1.2;
14 input real fsEps ("Conv. thresh. on feature step size");
15 input real geoEps ("Conv. thresh. on system geometry") = 0.1;
16 input real mvmtEps ("Conv. thresh. on point movement") = 0.01;
17 input real rpcEps ("Conv. thresh. on recent pop. changes") = 0.01;
18 input real pcpMeps ("Motion limit before PC") = 0.3;
19 input real isoval ("Which isosurface to sample") = 0;
20 input int verb ("Verbosity level") = 0;
21 input real sfs ("Scaling (<=1 for stability) on fStep") = 0.5;
22 input real hist ("How history matters for convergence") = 0.5;
23 // higher hist: slower change, more stringent convergence test
24 input int pcp ("periodicity of population control (PC)") = 5;
25 input vec3[] ipos ("Initial point positions");
26 input image(3)[] vol ("data to analyze");
27
28 field#2(3)[] F = bspln3 @ clamp(vol);
29
30 // Isosurface-specificity limited to fDim and these 5 functions
31 int fDim = 2;
32 function vec3 fStep(vec3 x) =
33 | (isoval - F(x)) * ∇F(x) / (|∇F(x)| * ∇F(x));
34 function tensor[3,3] ffPerp(vec3 x) {
35 | vec3 norm = normalize(∇F(x));
36 | return identity[3] - norm ⊗ norm;
37 }
38 function real fStrength(vec3 x) = |∇F(x)|;
39 function real fMask(vec3 x) = F(x);
40 function bool fTest(vec3 x) = true;
41
42 function bool posTest(vec3 x) =
43 | (inside(x, F) // in field
44 | && fStrength(x) > fStrTh // possibly near feature
45 | && fMask(x) >= fMaskTh // meets feature mask
46 | && fTest(x)); // passes addtl feature criterion
47
48 // Each particle wants between nnmin and nnmax neighbors
49 int nnmin = 6 if (2==fDim) else 2 if (1==fDim) else 0;
50 int nnmax = 8 if (2==fDim) else 3 if (1==fDim) else 0;
51
52 /* Potential function (found with Mathematica) phi(r):
53 | phi(0)=1, phi(r)=0 for r >= 1, with minima (potential well)
54 | phi'(2/3)=0 and phi(2/3)=-0.001. Phi(r) is C^3
55 | continuous across the well and with 0 for r >= 1. Potential
56 | well induces good packing with energy minimization. */
57 function real phi(real r) {
58 | real s=r-2.0/3;
59 | return
60 | | 1 + r*(-5.646 + r*(11.9835 + r*(-11.3535 + 4.0550625*r)))
61 | | if r < 2.0/3 else
62 | | | -0.001 + ((0.09 + (-0.54 + (1.215 - 0.972*s)*s)*s)*s)*s
63 | | if r < 1 else 0;
64 }
65 function real phi'(real r) { // phi'(r) = d phi(r) / dr
66 | real t=3*r-2;
67 | return
68 | | -5.646 + r*(23.967 + r*(-34.0605 + 16.22025*r))
69 | | if r < 2.0/3 else
70 | | | 0.01234567901*t*(4.86 + t*(-14.58 + t*(14.58 - 4.86*t)))
71 | | if r < 1 else 0;
72 }
73 real phiWellRad = 2/3.0; // radius of potential well
74 real rad = tipd/phiWellRad; // actual radius of potential support
75 function real enr(vec3 x) = phi(|x|/rad);
76 function vec3 frc(vec3 x) = phi'(|x|/rad) * (1/rad) * x/|x|;
77
78 // pchist reflects periodicity of PC: pchist^(2*pcp) = hist
79 real pchist = hist^(1.0/(2*pcp));
80
81 int iter = 0; // iteration counter
82 real rpc = 1; // recent population change
83 int popLast = -1; // population at last iteration

```

```

84 /* Finds a number in [0,1) roughly proportional to the low 32
   bits of significand of given real x. NOTE: ONLY useful only
   when compiling with --double */
85 function real urnd(real x) {
86 | if (x==0) return 0;
87 | real l2 = log2(|x|);
88 | real frxp = 2^(l2-floor(l2)-1); // in [0.5,1.0), like frexp(x)
89 | // use iter to make different values for same x
90 | return fmod((2^20 + 2*iter)*frxp, 1);
91 }
92
93 // Given vec3 (and iter), a random-ish value uniformly in [0,1)
94 function real v3rnd(vec3 v) {
95 | = fmod(urnd(v[0]) + urnd(v[1]) + urnd(v[2]), 1);
96
97 // Given vec3 (and iter), a big random-ish integer
98 function real genID(vec3 v) = floor(1000000*v3rnd(v));
99
100 // Is this an iteration in which to do population control (PC)?
101 | If not, pcIter() returns 0. Otherwise, returns 1 when should
102 | birth new particles, and -1 when should kill them off. This
103 | alternation is not due to any language limitations; it just
104 | plays well with the PC heuristics used here. */
105 function int pcIter() = ((iter%pcp)%2)*2 - 1
106 | if (pcp>0 && iter>0 && 0 == iter % pcp)
107 | | else 0;
108
109 // Strands first find feature, then interact w/ or make neighbors
110 strand point (vec3 p0, real hh0) {
111 | output vec3 pos = p0; // current particle position
112 | real ID = genID(p0); // strand identifier
113 | real hh = hh0; // energy gradient descent stepsize
114 | vec3 step = [0,0,0]; // energy+feature steps this iter
115 | bool found = false; // whether feature has been found
116 | int nfs = 0; // number feature steps taken
117 | real trav = 0; // total distance traveled
118 | real mvmt = 1; // average of recent movement
119 | real closest = rad; // distance to closest neighbor
120 | int born = 0; // how many particles I have birthed
121 | bool first = true; // first time through update
122 | update {
123 | | if (!posTest(pos)) {
124 | | | die;
125 | | }
126 | | if (travMax > 0 && trav > travMax) { // too much travel
127 | | | die;
128 | | }
129 | | if (!found) { // ----- looking for feature
130 | | | if (nfsMax > 0 && nfs > nfsMax) { // too many steps
131 | | | | die;
132 | | | }
133 | | | step = sfs*fStep(pos); // one step towards feature
134 | | | pos += step;
135 | | | mvmt = lerp(|step|/tipd, mvmt, hist);
136 | | | if (mvmt > fsEps) { // still moving
137 | | | | trav += |step|/tipd;
138 | | | | nfs += 1;
139 | | | } else { // found feature, prepare for code below
140 | | | | found = true;
141 | | | | mvmt = 1;
142 | | | | trav = 0;
143 | | | }
144 | | | if (found) { // ----- feature found; minimize energy
145 | | | | // if feature is isolated points, we're already done
146 | | | | if (0 == fDim) { stabilize; }
147 | | | | step = sfs*fStep(pos); pos += step; trav += |step|/tipd;
148 | | | | real oldE = 0; // energy at current location
149 | | | | vec3 force = [0,0,0]; // force on me from neighbors
150 | | | | int nn = 0; // number of neighbors
151 | | | | foreach (point P in sphere(rad)) {
152 | | | | | vec3 off = P.pos - pos;
153 | | | | | if (off/|tipd| < fsEps && P.ID <= P.ID) {
154 | | | | | | // with 0-D features or unlucky initialization, points
155 | | | | | | // can really overlap; point w/ lower ID dies
156 | | | | | | die;
157 | | | | | }
158 | | | | | oldE += enr(off);
159 | | | | | force += frc(off);
160 | | | | | nn += 1;
161 | | | | }
162 | | | | if (0 == nn) { // else fDim is 1 or 2
163 | | | | // No neighbors; create one if possible
164 | | | | if (!pcIter() > 0 && born < nnmax) { continue; }
165 | | | | // Ensure new pos is near feature, for all
166 | | | | // feature dimensions and orientations
167 | | | | vec3 noff0 = ffPerp(pos)•[tipd,0,0];
168 | | | | vec3 noff1 = ffPerp(pos)•[0,tipd,0];
169 | | | | vec3 noff2 = ffPerp(pos)•[0,0,tipd];
170 | | | | vec3 noff = noff0;
171 | | | }
172 }
173 }

```

```

174 noff = noff if |noff| > |noff1| else noff1;
175 noff = noff if |noff| > |noff2| else noff2;
176 // noff is now longest of noff0, noff1, noff2
177 vec3 npos = tipd*normalize(noff) + pos;
178 npos += sfs*fStep(npos);
179 if (posTest(pos)) {
180     | new point(npos, hh); born += 1;
181 }
182 continue;
183 }
184 // Else I did have neighbors; interact with them
185 vec3 es = hh*fPerp(pos)*force; // energy step along force
186 if (lesl > tipd) { // limit motion to tipd
187     hh *= tipd/lesl; // decrease stepsize, step
188     es *= tipd/lesl;
189 }
190 es *= 0.5; // now |es| <= tipd
191 vec3 fs = sfs*fStep(pos+es); // step towards feature
192 if (|fs|/(fsEps*tipd + |es|) > 0.5) {
193     hh *= 0.5; // feature step too big, try w/ smaller step
194     continue;
195 }
196 vec3 oldpos = pos;
197 pos += fs + es; // take steps, find new energy
198 real newE = 0;
199 closest = rad;
200 // find mean neighbor offset (mno) to know (opposite)
201 // direction in which to add new particles with PC
202 vec3 mno = [0,0,0];
203 nn = 0;
204 foreach (point P in sphere(rad)) {
205     vec3 off = P.pos - pos;
206     newE += enr(off);
207     closest = min(closest, |off|);
208     mno += off;
209     nn += 1;
210 }
211 mno /= nn;
212 // test the Armijo sufficient decrease condition
213 if (newE - oldE > gdeTest*(pos - oldpos)*(-force)) {
214     // backtrack because energy didn't go down enough
215     hh *= gdeBack; // try again next time w/ smaller step
216     if (0 == hh) {
217         die; // backtracked all the way to hh=0!
218     }
219     pos = oldpos;
220     continue;
221 }
222 hh *= gdeOppor; // opportunistically increase stepsize
223 step += fs + es;
224 trav += |step|/tipd;
225 mvmt = lerp(|step|/tipd, mvmt, hist);
226 if (|step|/tipd < pcmtEps && pcIter() != 0) {
227     // can do PC only if haven't moved a lot
228     if (pcIter()>0 // this is an iter to add
229         && newE<0 // already in a potential well
230         && nn<nnmin // have fewer than expected neighbors
231         && born<nnmax) { // haven't birthed too many times
232         vec3 npos = pos - tipd*normalize(mno);
233         npos += sfs*fStep(npos); npos += sfs*fStep(npos);
234         bool birth = true;
235         if (fDim == 2 && nn >= 4) {
236             foreach (point P in sphere(npos, tipd*mab)) {
237                 birth = false; // too close to existing point
238             }
239             if (birth) {
240                 // Have nn neighbors: too few (nnmin > nn).
241                 // Try adding a new neighbor with a probability
242                 // that scales with nnmin-nn.
243                 birth = v3rnd(pos) < (nnmin - nn)/real(nnmin);
244             }
245             if (birth && posTest(npos)) {
246                 | new point(npos, hh); born += 1;
247             }
248         } else if (pcIter() < 0 && newE > 0 && nn > nnmax) {
249             // Have too many neighbors, so maybe die. If I have
250             // nn neighbors, they probably also have nn neighbors.
251             // To have fewer, that is, nnmax neighbors, we all
252             // die with chance of nn-nnmax out of nn.
253             if (v3rnd(pos) < (nn - nnmax)/real(nn)) {
254                 die;
255             }
256         }
257     }
258 } // else found
259 first = false;
260 } // update
261 }
262 global {
263     int pop = numActive();
264
265     int pc = 1 if pop != popLast else 0;
266     rpc = lerp(pc, rpc, pchist);
267     bool allfound = all { P.found | P in point.all};
268     real percfound =
269         100* mean { 1.0 if P.found else 0.0 | P in point.all};
270     real meancl = mean { P.closest | P in point.all };
271     real varic1 = mean { (P.closest - meancl)^2 | P in point.all };
272     real covcl = sqrt(varic1) / meancl;
273     real maxmvmt = max { P.mvmt | P in point.all };
274     print("===== finished iter ", iter, " w/ ", pop, ")");
275     "; %found=", percfound,
276     "; mean(hh)=", mean { P.hh | P in point.all},
277     "; mean(c1)=", meancl,
278     "; COV(c1)=", covcl,
279     "; max(mvmt)=", maxmvmt,
280     "; pc=", pc,
281     "; rpc=", rpc,
282     "\n");
283 if (allfound // all particles have found the feature
284     && covcl < geoEps // and system is geometrically uniform
285     && maxmvmt < mvmtEps // and nothing's moving much
286     && rpc < rpcEps) { // and pop. hasn't changed recently
287     print("===== Stabilizing ", numActive(), " (iter ", iter, "),
288     "; COV(c1)=", covcl, " < ", geoEps,
289     "; max(mvmt)=", maxmvmt, " < ", mvmtEps,
290     "; rpc=", rpc, " < ", rpcEps,
291     "\n");
292 }
293 iter += 1;
294 popLast = pop;
295 }
296 initially { point(ipos[iil], 1) | ii in 0 .. length(ipos)-1 };

```

As with the direct volume renderer, the code specific to one feature is isolated to one place: the statement of feature dimension fDim (line 31), and the feature functions starting on line 32. Relative to the renderer, the new feature function is fPerp (line 34), which projects onto the orthogonal complement of the possible local feature steps.

Compared with the basic particle system program (Fig. 4), the program is longer and more complex, but the basic structure is the same. There is still a univariate inter-particle potential energy $\phi(r)$, is implemented as phi (line 57), which is a piecewise polynomial with a slight potential well at $r = 2/3$. The function is graphed in

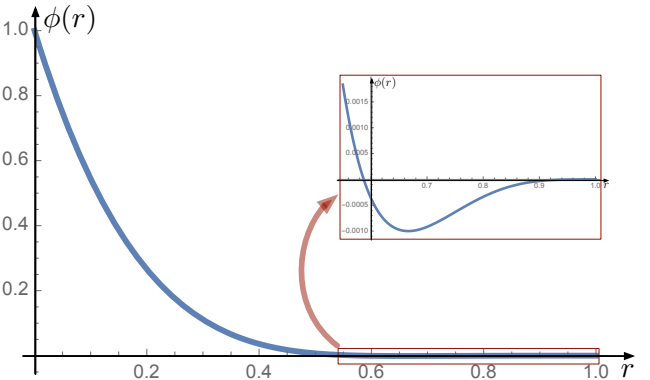


Figure 9: Graph of inter-particle potential function $\phi(r)$

Fig. 9, which includes an inset that vertically expands the plot over interval $[0.55, 1]$ to clarify the location and shape of the potential well. The relative shallowness of the potential well compared to height at $r = 0$ ensures that energy minimization separates close particles before it attempts to produce uniform spacing.

The functions over 3D space for energy (enr on line 75) and force (frc on line 76) are defined as they were in simple Fig. 4

program. The control of the population of the particle system is probabilistic in flavor, using function `v3rnd` (line 97) which generates from a `vec3 v` a value in $[0, 1]$ by combining the low-order bits of the X, Y, and Z coordinates of `v` (as exposed by `urnd` on line 88) with the current program iteration count. The current version of Diderot lacks a pseudo-random number generator. The same `v3rnd` is used in the `genID` function (line 101) used to assign to each strand a number (hopefully unique), which proves useful for debugging. A unique per-strand identifier that is thread-safe and stable across iterations is currently not available in Diderot. The periodicity of considering to add or kill particles is controlled by `pcIter` (line 108).

As in the simple particle system (Fig. 4), each program strand computes the position of one particle. Each particle starts (with `found=false`, line 118) looking for the feature of interest with repeated `fSteps` (lines 132 through 146) while ignoring other particles, after which (lines 147 through 258) particles interact with each other to produce a uniform feature sampling. This second phase includes careful mechanisms for population control. If particles have no neighbors (lines 165 through 183), an effort is made to create a new neighbor close to the feature, using `fPerp`. Computing energy at the updated location (lines 203 through 210) includes computing a mean offset to neighbors `mno`, which is used later (line 231) as part of determining where to try add a new particle in case of under-population. Because the $\phi(r)$ function in the minimal Fig. 4 particle system program was purely repulsive, the last energy gradient descent direction could play that role (Fig. 4 line 73), but here the $\phi(r)$ includes a potential well, so the geometric information in `mno` is useful. If the particle has not predictably moved downhill in energy (line 212), it backtracks and tries again on the next iteration.

Otherwise (line 221), with predictable energy descent, the records of recent motion are updated (line 222), and, if recent motion is small, population control is considered (local estimates of particle density mean less if the system is rapidly moving). Precautions are taken to ensure that the intended location of the a new particle are not too close to an existing one, via the minimum allowed birth distance `mabd` parameter (input line 7, used line 235). This parameter is subtle: if too high, significant holes are never filled in, and if too low, then the pentagonal arrangements of points

that may appropriately minimize energy on higher curvature surfaces may trigger the birth of multiple particles, each trying to create a local hexagonal packing (wherein every particle will see $nn_{min} = 6$ neighbors). Fig. 10 illustrates the geometric reasoning involved in setting `mabd`. If particles, separated by S , have formed a pentagon, then if one adds a new particle at distance S , it will have distance D from another particle on the other side of the pentagon; $D/S \approx 0.735085$. Setting `mabd` higher than this (0.75 works in our experience) prevents pentagonal holes from triggering excessive births. Subsequent meshing can fill the whole by adding two edges and three triangles.

The chances of creating a new particle (if the `mabd` test passes, line 242) or of a particle exiting the computation (line 253) depend on the relationship between the number of neighbors `nn` and the target range of neighbor numbers `[nnmin,nnmax]`. The intent is that after one or two periods of population control, the system has roughly the correct number of particles and can proceed to distribute them in a uniform way. While this code with these parameter settings worked adequately to produce our current results, we hope that further computational and geometric analysis can demonstrate the theoretical stability and robustness of the method.

In the final part of the program, the global update (line 262), the particle system state is measured to test for convergence (line 282), which includes tests on the recent stability of particle position and number, as well as their spatial uniformity, as measured by the coefficient-of-variation of distances to interacting neighbors.

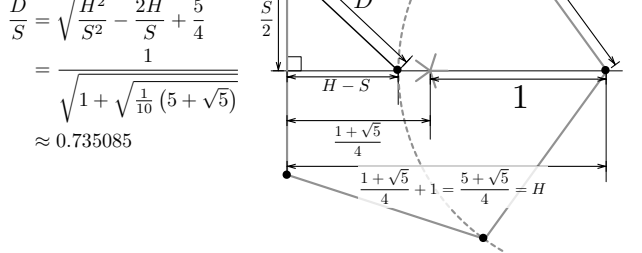


Figure 10: Geometric derivation of lower bound on `mabd` parameter to avoid filling pentagonal holes in sampling

Appendix C: Human-readable Diderot intermediate representation

The ability of the Diderot compiler to generate code that computes higher-order derivatives of vector and tensor fields has enabled our work to date. How any compiler converts the surface programming language into working code requires multiple stages of internal or intermediate representation. We thought it might be interesting to see what the Diderot compiler is doing with the expressions associated with extremal features, by modifying the (open-source) compiler to print some of its intermediate representations. We show here human-readable expressions for gradient and Hessian of the Parallel Vector Operator used for many vector field features [PR99].

If we consider two 3D vector fields $\mathbf{a}(\mathbf{x})$ and $\mathbf{b}(\mathbf{x})$ (these two letters are more easily distinguished than the standard $\mathbf{u}(\mathbf{x})$ and $\mathbf{v}(\mathbf{x})$), the Parallel Vector Operator (PVO) $\mathbf{a} \parallel \mathbf{b}$ is true at points \mathbf{x} where $\mathbf{a}(\mathbf{x})$ is parallel to $\mathbf{b}(\mathbf{x})$, i.e.

$$(\mathbf{a} \parallel \mathbf{b})(\mathbf{x}) \Leftrightarrow P(\mathbf{x}) = \frac{\mathbf{a}(\mathbf{x})}{|\mathbf{a}(\mathbf{x})|} \cdot \frac{\mathbf{b}(\mathbf{x})}{|\mathbf{b}(\mathbf{x})|} = \pm 1 \quad (24)$$

Our approach to visualizing or extracting $\mathbf{a} \parallel \mathbf{b}$ involves finding the Newton step towards $\mathbf{a} \parallel \mathbf{b}$. Since $\mathbf{a} \parallel \mathbf{b}$ are particular ridge and valley lines of $\mathbf{a} \cdot \mathbf{b}/(|\mathbf{a}| |\mathbf{b}|)$ (where the height is $+1$ and -1 , respectively), we need the gradient and Hessian of $(\mathbf{a}/|\mathbf{a}|) \cdot (\mathbf{b}/|\mathbf{b}|)$ to compute the Newton step with (12) of Sec. 2.1.

We were able to modify the open-source Diderot compiler to learn expressions for these derivatives, by printing L^AT_EXor Unicode formatings of the intermediate representation. Starting with a minimal program to evaluate once the gradient of the PVO:

```

1 input image(3)[3] A;
2 input image(3)[3] B;
3 field#2(3)[3] a = bspln3 ⊗ A;
4 field#2(3)[3] b = bspln3 ⊗ B;
5
6 field#2(3)[] P = (a/|a|)•(b/|b|); // the PVO
7
8 strand f(int i) {
9 |   output tensor[3] r = ∇P([0,0,0]);
10 |   update {
11 |   |   stabilize;
12 |   }
13 }
14 initially [ f(i) | i in 0..0];

```

$$\begin{aligned}
& \frac{((\nabla \otimes A)^T \bullet \nabla \otimes B) + (A \bullet \nabla \otimes \nabla \otimes B) + ((\nabla \otimes B)^T \bullet \nabla \otimes A) + (B \bullet \nabla \otimes \nabla \otimes A)}{(|B| * |A|)} \\
& + \frac{(((B \bullet A) * ((A \bullet \nabla \otimes A) \otimes (A \bullet \nabla \otimes A))) + (2 * (B \bullet A) * ((A \bullet \nabla \otimes A) \otimes (A \bullet \nabla \otimes A))))}{(|B| * |A| * (A \bullet A))^2} \\
& + \frac{(((B \bullet A) * ((B \bullet \nabla \otimes B) \otimes (A \bullet \nabla \otimes A))) + ((B \bullet A) * ((A \bullet \nabla \otimes A) \otimes (B \bullet \nabla \otimes B))))}{((B \bullet B) * |A| * |B| * (A \bullet A))} \\
& + \frac{((B \bullet A) * ((B \bullet \nabla \otimes B) \otimes (B \bullet \nabla \otimes B))) + (2 * |B| * (B \bullet A) * ((B \bullet \nabla \otimes B) \otimes (B \bullet \nabla \otimes B)))}{(|B| * |A| * (B \bullet B))^2} \\
& - \frac{(((A \bullet \nabla \otimes A) \otimes (B \bullet \nabla \otimes A)) + (((A \bullet \nabla \otimes A) \otimes (A \bullet \nabla \otimes B))) + ((B \bullet A) * ((\nabla \otimes A)^T \bullet \nabla \otimes B)) + ((B \bullet A) * (A \bullet \nabla \otimes \nabla \otimes A)) + (((A \bullet \nabla \otimes B) \otimes (A \bullet \nabla \otimes A)) + (((B \bullet \nabla \otimes A) \otimes (A \bullet \nabla \otimes A))))}{(|B| * |A| * (A \bullet A))} \\
& + \frac{(((B \bullet \nabla \otimes B) \otimes (B \bullet \nabla \otimes A)) + (((A \bullet \nabla \otimes B) \otimes (B \bullet \nabla \otimes B)) + (((B \bullet \nabla \otimes B) \otimes (A \bullet \nabla \otimes B)) + (((B \bullet \nabla \otimes A) \otimes (B \bullet \nabla \otimes B))))}{(|A| * |B| * (B \bullet B))} \\
& + \frac{((|B| * (B \bullet A) * ((\nabla \otimes B)^T \bullet \nabla \otimes B)) + (|B| * (B \bullet A) * (B \bullet \nabla \otimes \nabla \otimes B)))}{(|A| * (B \bullet B) * (B \bullet B))}
\end{aligned}$$

Our modified compiler generated:

$$\frac{((A \bullet \nabla \otimes B) + (B \bullet \nabla \otimes A))}{(|A| * |B|)} \quad (25)$$

$$- \frac{((B \bullet A) * ((A \bullet \nabla \otimes A))) + ((B \bullet A) * (B \bullet \nabla \otimes B))}{(|A| * |B| * (A \bullet A))} + \frac{((B \bullet A) * ((B \bullet \nabla \otimes B)))}{(|B| * |A| * (B \bullet B))}, \quad (26)$$

which we manually post-processed to find:

$$\nabla P = \frac{\mathbf{a} \cdot \nabla \otimes \mathbf{b} + \mathbf{b} \cdot \nabla \otimes \mathbf{a} - \mathbf{a} \cdot \mathbf{b} \left(\frac{\mathbf{a} \cdot \nabla \otimes \mathbf{a}}{\mathbf{a} \cdot \mathbf{a}} + \frac{\mathbf{b} \cdot \nabla \otimes \mathbf{b}}{\mathbf{b} \cdot \mathbf{b}} \right)}{|\mathbf{a}| |\mathbf{b}|}. \quad (27)$$

We were not previously familiar with this expression of ∇P , which (to first order) points towards (or away from) where \mathbf{a} and \mathbf{b} are parallel. Terms like $\mathbf{a} \cdot \nabla \otimes \mathbf{b}$ are the Jacobian $\nabla \otimes \mathbf{b}$ of \mathbf{b} , contracted on the left by \mathbf{a} , which can be thought of as a sum over the rows of $\nabla \otimes \mathbf{b}$, weighted by the components of \mathbf{a} . The ∇P expression could also be derived by hand, but it was a nearly automatic side-effect of our modified Diderot compiler. The expression for ∇P is symmetric in switching \mathbf{a} and \mathbf{b} , which is reassuring.

For comparison, Van Gelder and Pang, also interested in iterative methods to extract PVO features, derive (with a page of careful explanation) this condition for a step $\mathbf{\epsilon}$ from \mathbf{x} such that $\mathbf{x} + \mathbf{\epsilon}$ satisfies $\mathbf{a} \parallel \mathbf{b}$ (c.f. (29) in [GP09]):

$$\begin{aligned}
& \mathbf{q} + \left(\mathbf{I} - \frac{\mathbf{b} \otimes \mathbf{b}}{\mathbf{b} \cdot \mathbf{v}} \right) (\nabla \otimes \mathbf{a} - s \nabla \otimes \mathbf{b}) \mathbf{\epsilon} \\
& - \left(\frac{\mathbf{b} \otimes \mathbf{q}}{\mathbf{b} \cdot \mathbf{b}} \nabla \otimes \mathbf{b} + \frac{\mathbf{q} \otimes \mathbf{a}}{\mathbf{a} \cdot \mathbf{a}} \nabla \otimes \mathbf{a} \right) \mathbf{\epsilon} = \mathbf{0}
\end{aligned} \quad (28)$$

where

$$\mathbf{q} = \left(\mathbf{I} - \frac{\mathbf{b} \otimes \mathbf{b}}{\mathbf{b} \cdot \mathbf{b}} \right) \mathbf{a} \quad (29)$$

is the component of \mathbf{a} orthogonal to \mathbf{b} . The authors then describe how $\mathbf{\epsilon}$ may then be computed as the solution to a system of equations as part of an iterative search. They chose a mathematical formulation that is not symmetric in switching \mathbf{a} and \mathbf{b} .

We were curious if our modified Diderot compiler could produce a human-readable expression for the Hessian of $P(\mathbf{x}) = \frac{\mathbf{a}(\mathbf{x})}{|\mathbf{a}(\mathbf{x})|} \cdot \frac{\mathbf{b}(\mathbf{x})}{|\mathbf{b}(\mathbf{x})|}$, which is inverted as to compute, via (12), the feature step of our approach. By changing line 9 in the program above to include $r = \nabla \otimes \nabla P([0,0,0])$; our modified compiler generated a lengthy expression:

With some manual post-processing (factoring common terms and regrouping), we develop an expression for the Hessian of P :

$$\nabla \otimes \nabla P = \frac{(\nabla \otimes \mathbf{b})^T \cdot \nabla \otimes \mathbf{a} + (\nabla \otimes \mathbf{a})^T \cdot \nabla \otimes \mathbf{b} + \mathbf{a} \cdot \nabla \otimes \nabla \otimes \mathbf{b} + \mathbf{b} \cdot \nabla \otimes \nabla \otimes \mathbf{a}}{|\mathbf{a}| |\mathbf{b}|} + \frac{\mathbf{a} \cdot \mathbf{b} \left(\frac{3(\mathbf{b} \cdot \nabla \otimes \mathbf{b}) \otimes (\mathbf{b} \cdot \nabla \otimes \mathbf{b})}{(\mathbf{b} \cdot \mathbf{b})^2} + \frac{3(\mathbf{a} \cdot \nabla \otimes \mathbf{a}) \otimes (\mathbf{a} \cdot \nabla \otimes \mathbf{a})}{(\mathbf{a} \cdot \mathbf{a})^2} + \frac{(\mathbf{a} \cdot \nabla \otimes \mathbf{a}) \otimes (\mathbf{b} \cdot \nabla \otimes \mathbf{b}) + (\mathbf{b} \cdot \nabla \otimes \mathbf{b}) \otimes (\mathbf{a} \cdot \nabla \otimes \mathbf{a})}{(\mathbf{a} \cdot \mathbf{a})(\mathbf{b} \cdot \mathbf{b})} \right)}{|\mathbf{a}| |\mathbf{b}|} - \frac{\mathbf{a} \cdot \mathbf{b} (\mathbf{b} \cdot \nabla \otimes \nabla \otimes \mathbf{b} + (\nabla \otimes \mathbf{b})^T \cdot \nabla \otimes \mathbf{b}) + (\mathbf{a} \cdot \nabla \otimes \mathbf{b} + \mathbf{b} \cdot \nabla \otimes \mathbf{a}) \otimes (\mathbf{b} \cdot \nabla \otimes \mathbf{b}) + (\mathbf{b} \cdot \nabla \otimes \mathbf{b}) \otimes (\mathbf{a} \cdot \nabla \otimes \mathbf{b} + \mathbf{b} \cdot \nabla \otimes \mathbf{a})}{\mathbf{b} \cdot \mathbf{b}} - \frac{\mathbf{a} \cdot \mathbf{b} (\mathbf{a} \cdot \nabla \otimes \nabla \otimes \mathbf{a} + (\nabla \otimes \mathbf{a})^T \cdot \nabla \otimes \mathbf{a}) + (\mathbf{a} \cdot \nabla \otimes \mathbf{b} + \mathbf{b} \cdot \nabla \otimes \mathbf{a}) \otimes (\mathbf{a} \cdot \nabla \otimes \mathbf{a}) + (\mathbf{a} \cdot \nabla \otimes \mathbf{a}) \otimes (\mathbf{a} \cdot \nabla \otimes \mathbf{b} + \mathbf{b} \cdot \nabla \otimes \mathbf{a})}{\mathbf{a} \cdot \mathbf{a}}$$

(30)

Review of this expression reveals that it too is symmetric in switching \mathbf{a} and \mathbf{b} . $\nabla \otimes \nabla \otimes \mathbf{a}$ is the Hessian of vector field \mathbf{a} , a third-order tensor that, when right multiplied by offset $\boldsymbol{\epsilon}$, gives the local change in the Jacobian. While it would also be possible to derive $\nabla \otimes \nabla P$ by hand, the automated operation of a compiler may be more trustworthy. We show this expression for $\nabla \otimes \nabla P$ to demonstrate functionality that is otherwise hidden inside the Diderot compiler, and to document a complicated formula that others may find useful if implementing Newton steps towards PVO features without Diderot.

Appendix D: Utility programs in Diderot

We we include, for the sake of completeness, other Diderot programs and functions that were used to compute results or generate figures.

D.1. Finding 1D column-space (`col1span`)

```

1 // finds vector spanning 1D columnspace
2 function vec3 col1span(tensor[3,3] m) {
3     vec3 ret = [0,0,0];
4     vec3 c0 = m[:,0]; // extract columns
5     vec3 c1 = m[:,1];
6     vec3 c2 = m[:,2];
7     vec3 c = c0;
8     // learn which column is longest
9     int which = 0;
10    if (|c1| > |c|) { c = c1; which = 1; }
11    if (|c2| > |c|) { c = c2; which = 2; }
12    // starting with longest column, add in other columns,
13    // negating as needed to get longest (most accurate) sum
14    if (0 == which) {
15        ret = c0;
16        ret += c1 if c1*c0 > 0 else -c1;
17        ret += c2 if c2*c0 > 0 else -c2;
18    } else if (1 == which) {
19        ret = c1;
20        ret += c0 if c0*c1 > 0 else -c0;
21        ret += c2 if c2*c1 > 0 else -c2;
22    } else { // 2 == which
23        ret = c2;
24        ret += c0 if c0*c2 > 0 else -c0;
25        ret += c1 if c1*c2 > 0 else -c1;
26    }
27    // normalize result if possible
28    return normalize(ret) if |ret|>0 else [0,0,0];
29 }
```

The above function is used as part of surface crease line rendering (Sec. 4.3), to find the single eigenvector of a symmetric 3×3 matrix associated with the sole non-zero eigenvalue. This amounts to finding a vector that spans the column space of the matrix, which the above function does by finding the longest possible sum of (possibly negated) columns in the given matrix, and then normalizing.

D.2. Finding edges between particles (`edge.diderot`)

```

1 input vec3{} ipos ("vertex positions") = load("pos.nrrd");
2 input real rad ("radius within which verts are edge-connected");
3
4 strand point (int ii, vec3 pp) {
5     // the output of this program is what it print(),s,
6     // rather than this "output" variable foo.
7     output real foo=0;
8     int ID = ii; // record our index in vert list
9     vec3 pos = pp; // record spatial position
10    update {
11        // the sphere() test implicitly depends on pos
12        foreach (point P in sphere(rad)) {
13            if (ID < P.ID) {
14                // only report each edge once
15                print(ID, "\n", P.ID, "\n");
16            }
17        }
18        stabilize;
19    }
20 }
21
22 initially { point(ii, ipos[ii]) | ii in 0 .. length(ipos)-1 };
```

The above utility program is used for the first stage of meshing feature sampling results systems (Sec. 3.3): connecting neighboring vertices together. Because the particle system tends to produce very uniform samplings at and near convergence, the test for whether two vertices (as represented by two particles) should be considered edge-connected is reduced to knowing if they interacted in the last iteration. Because for this work we have not yet attempted to vary sampling density based on feature characteristics, this is in turn

equivalent to asking whether two particles are within the potential function $\phi(r)$ support of each other. Assuming the $\phi(r)$ described in Appendix B, with its potential well at $r = 2/3$, the radius `rad` given to on line 2 should be $3/2$ of the target inter-particle distance (`tipd`, Appendix B line 4) used for particle system computation. A k-d tree created by Diderot run-time based on the special `pos` position variable (line 9) ensures that the `sphere` test (line 12) is executed efficiently.

D.3. PostScript mesh drawing (`epsdraw.diderot`)

The program below is included for the sake of completeness since it is used for figure generation (Fig 1 bottom row, Fig. 3(b,c,d), and Fig. 5). It produces a PostScript depiction of small particle systems and their meshes, by computing world-to-view and view-to-screen transformations via homogeneous coordinates. With its ability to label all edges, vertices, and faces in a vector graphics output, it was used for debugging the Appendix B particle system program, and its subsequent meshing. This is not, however, a typical or especially informative Diderot program. Like `edge.diderot` above, the useful output of this program is via its many `print` statements, rather than typical per-strand computed output. Diderot currently has no means of sorting strands based on computed results, so the PostScript commands to draw each element are printed to a single line of text, which starts with “Z pop” where Z is screen depth. Sorting these lines as a post-process ensures that PostScript will draw closer elements after (on top of) further elements.

```

1 input vec3{} ipos ("point positions");
2 input int{} edg ("edges as pairs of point indices");
3 input int{} tri ("triangles as triplets of point indices");
4 int ptNum = length(ipos);
5 int edgNum = 0 if (edg[0] == 0 && edg[1] == 0)
6     else length(edg)/2;
7 int triNum = 0 if (tri[0] == 0 && tri[1] == 0 && tri[2] == 0)
8     else length(tri)/3;
9
10 input image(3)[] img ("data to analyze") = image("vol.nrrd");
11 input vec3 camEye ("camera look-from point") = [6, 9, 2];
12 input vec3 camAt ("camera look-at point") = [0, 0, 0];
13 input vec2 clasuv ("Camera Look-at Shift at along U,V") = [0,0];
14 input vec3 camUp ("camera pseudo-up vector") = [0, 0, 1];
15 input real camNear ("at-relative near clip distance") = -3;
16 input real camFar ("at-relative far clip distance") = 3;
17 input real camFOV ("vertical field-of-view angle") = 15;
18 input bool camOrtho ("orthographic (not perspective)") = false;
19 input int iresU ("image # horizontal samples") = 640;
20 input int iresV ("image # vertical samples") = 480;
21 input real clwid ("circle line width (in world space!)") = 0.01;
22 input real elwid ("edge line width (in screen space!)") = 0.1;
23 input real revth ("draw reversed edges this much thicker") = 6;
24 input bool cfill ("should fill circle") = true;
25 input bool bvcull ("back vertex culling") = false;
26 input real lab ("if > 0, font size for labeling things") = 0;
27 input real crd ("circle radius");
28 input real drd ("dot radius");
29 input real frgray ("front-facing gray") = 0.3;
30 input real egray ("edge gray") = 0;
31 input real bkgray ("back-facing gray") = 0.8;
32 input real trigray ("triangle gray") = 0.8;
33 input real scl ("scaling") = 120;
34 /* this string identifies what kind of feature should be drawn,
   which matters for choosing how to determine the apparent
   orientation of the disc used to indicate each vertex */
35 input string feat ("FEAT-ISO, FEAT-RSF, FEAT-VSF, or FEAT-RLN");
36
37
38 // computing ray parameters and view-space basis
39 vec3 camN_ = normalize(camAt - camEye); // N: away from eye
40 vec3 camU_ = normalize(camN_ × normalize(camUp)); // U: right
41 vec3 camV_ = camN_ × camU_; // V: down
42 // now with camAtShift
43 vec3 camA_ = normalize(camAt + clasuv[0]*camU_
44                                + clasuv[1]*camV_ - camEye);
45 vec3 camU = normalize(camN × normalize(camUp));
46 vec3 camV = camN × camU;
47 real camDist = |camAt + clasuv[0]*camU_
48                                + clasuv[1]*camV_ - camEye|;
49 real camVmax = tan(camFOV*π/360)*camDist;
```

```

50 real camUmax = camVmax*iresU/iresV;
51 real camNearV = camNear + camDist; // near clip, view space
52 real camFarV = camFar + camDist; // far clip, view space
53
54 real hght = 2*camVmax;
55 real width = hght*iresU/iresV;
56
57 // determine view transforms
58 tensor[4,4] WtoV = [
59 [camU[0], camU[1], camU[2], -camU•camEye],
60 [camV[0], camV[1], camV[2], -camV•camEye],
61 [camN[0], camN[1], camN[2], -camN•camEye],
62 [0, 0, 0, 1]];
63 tensor[4,4] perspVtoC = [
64 [2*camDist/width, 0, 0, 0],
65 [0, 2*camDist/hght, 0, 0],
66 [0, 0, (camFarV+camNearV)/(camFarV-camNearV),
67 [-2*camFarV*camNearV/(camFarV-camNearV)],
68 [0, 0, 1, 0];
69 tensor[4,4] orthoVtoC = [
70 [2/width, 0, 0, 0],
71 [0, 2/hght, 0, 0],
72 [0, 0, 2/(camFarV-camNearV),
73 [-2*(camFarV+camNearV)/(camFarV-camNearV)],
74 [0, 0, 0, 1];
75 tensor[4,4] VtoC = orthoVtoC if camOrtho else perspVtoC;
76 tensor[4,4] CtoS = [
77 [scl*camUmax, 0, 0, 0],
78 [0, scl*camVmax, 0, 0],
79 [0, 0, 1, 0],
80 [0, 0, 0, 1];
81
82 field#2(3)[] F = bspln3 @ clamp(img);
83
84 // undo homogeneous coords
85 function vec3 unh(vec4 ch) =
86 | [ch[0]/ch[3], ch[1]/ch[3], ch[2]/ch[3]];
87 // convert to homogeneous coords
88 function vec4 hom(vec3 c) = [c[0], c[1], c[2], 1];
89 // how to approximate surface "normal"
90 function vec3 snorm(vec3 p) {
91 vec3 ret=[0,0,0];
92 if (feat == "FEAT-ISO") {
93 | ret = normalize(-∇F(p));
94 } else if (feat == "FEAT-RSF") {
95 | ret = evecs(∇⊗∇F(p))[2];
96 } else if (feat == "FEAT-VSF" || feat == "FEAT-RLN") {
97 | ret = evecs(∇⊗∇F(p))[0];
98 } else if (feat == "FEAT-CTP") {
99 | ret = -camN;
100 } else {
101 | ret = [nan,nan,nan];
102 }
103 return ret;
104 }
105 bool snsng = true if (feat == "FEAT-ISO") else
106 false if (feat == "FEAT-RSF") else
107 false if (feat == "FEAT-VSF") else
108 false if (feat == "FEAT-RLN") else
109 false;
110
111 strand draw (int ii) {
112 output real foo=0;
113 update {
114
115 // only one strand prints preamble
116 if (ii==0) {
117 print("%!PS-Adobe-3.0 EPSF-3.0\n");
118 print("%<Creator: Diderot\n");
119 print("%<Title: awesome figure\n");
120 print("%<Pages: 1\n");
121 print("%<BoundingBox: ", -scl*camUmax, " ", -scl*camVmax,
122 " ", scl*camUmax, " ", scl*camVmax, "\n");
123 print("%<EndComments\n");
124 print("%<BeginProlog\n");
125 print("%<EndProlog\n");
126 print("%<Page: 1 1\n");
127 print("gsave\n");
128 print(-scl*camUmax, " ", -scl*camVmax, " moveto\n");
129 print(scl*camUmax, " ", -scl*camVmax, " lineto\n");
130 print(scl*camUmax, " ", scl*camVmax, " lineto\n");
131 print(-scl*camUmax, " ", scl*camVmax, " lineto\n");
132 print("closepath\n");
133 print("gsave newpath\n");
134 print("1 -1 scale\n");
135 if (label > 0) {
136 | print("Times-Roman findfont\n");
137 | print(label, " scalefont setfont\n");
138 }
139
140 if (ii <= pntNum-1) {
141 /* */
142
143 // position of center of glyph to draw
144 q_ from p, in direction towards eye, but tangent
145 // (normal to normal); should get the most fore-shortening
146 r_ from p, in direction perpendicular to q's offset from p
147 _w: world-space coords
148 _s: screen-space coords
149 */
150 vec3 pw = ipos[ii];
151 vec3 nw = snorm(pw);
152 if (|nw| >= 0) {
153 // nn == Nothing along Normal
154 tensor[3,3] nn = identity[3] - nw⊗nw;
155 vec3 toeyp = normalize(camEye - pw);
156 vec3 qo = drd*normalize(nn•toeye);
157 vec3 qw = pw + qo;
158 vec3 ro = drd*normalize(nw×qo);
159 vec3 rw = pw + ro;
160 vec3 ps = unh(CtoS•VtoC•WtoV•hom(pw));
161 vec3 qs = unh(CtoS•VtoC•WtoV•hom(qw));
162 vec3 rs = unh(CtoS•VtoC•WtoV•hom(rw));
163 if (ps[2] && ps[2] <= 1
164 && (!snsng || !bcvull || nw•toeye > 0)) {
165 print(ps[2], " pop ");
166 print("gsave ");
167 print(ps[0], " ", ps[1], " translate ");
168 real gray = frgray if (!snsng) else
169 | frgray if (nw•toeye > 0) else bkgray;
170 vec3 rso = [[1,0,0],[0,1,0],[0,0,1]]•(rs - ps);
171 vec3 qso = [[1,0,0],[0,1,0],[0,0,1]]•(qs - ps);
172 print(180*atan2(rso[1],rso[0])/\pi, " rotate ");
173 print(rso, " ", qso, " scale ");
174 print(gray, " setgray ");
175 if (clwid > 0) {
176 print(clwid/drd, " setlinewidth ");
177 print("0 0 ", crd/dr, " 0 360 arc closepath ");
178 if (ccfill) { print("gsave 1 setgray fill grestore "); }
179 print("stroke ");
180 if (frgray == gray) {
181 | print("0 0 1 0 360 arc closepath fill ");
182 } else {
183 print("0 0 1 0 360 arc closepath fill ");
184 }
185 print("grestore ");
186 print("% vi=", ii, "\n");
187 if (label > 0) {
188 print(ps[2]-0.1, " pop gsave 0.5 setgray newpath ",
189 ps[0], " ", ps[1],
190 " moveto 1 -1 scale (v", ii, ") show grestore\n");
191 }
192 }
193 }
194 } else if (ii <= pntNum+edgNum-1) {
195 int ei=ii-pntNum; // edge index
196 int pi0 = edg[0 + 2*ei];
197 int pil = edg[1 + 2*ei];
198 if (pi0 != pil) {
199 vec3 pw0 = ipos[pi0];
200 vec3 pw1 = ipos[pil];
201 vec3 nw0 = snorm(pw0);
202 vec3 nw1 = snorm(pw1);
203 if (|nw0| >= 0 && |nw1| >= 0) {
204 vec3 toeyp0 = normalize(camEye - pw0);
205 vec3 toeyp1 = normalize(camEye - pw1);
206 if (!snsng || (toeyp0•nw0 > 0 && toeyp1•nw1 > 0)) {
207 vec3 ps0 = unh(CtoS•VtoC•WtoV•hom(pw0));
208 vec3 ps1 = unh(CtoS•VtoC•WtoV•hom(pw1));
209 real ez = min(ps0[2], ps1[2]);
210 if (-1 <= ez && ez <= 1) {
211 | print(ez, " pop ");
212 | print(egray, " setgray ",
213 | | elwid*(1 if pi0 < pil else revth),
214 | | " setlinewidth ",
215 | | ps0[0], " ", ps0[1], " moveto ", ps1[0],
216 | | " ", ps1[1], " lineto stroke % ei=",
217 | | ei, "\n");
218 | if (label > 0) {
219 | | print(ez-0.1, " pop ");
220 | | vec3 ms = lerp(ps0, ps1, 0.5);
221 | | print("gsave 0.5 setgray newpath ", ms[0],
222 | | " ", ms[1], " moveto (e", ei,
223 | | " ) 1 -1 scale show grestore\n");
224 | | }
225 | }
226 | }
227 | }
228 }
229 } else {
230 int ti = ii-pntNum-edgNum; // tri index
231 int pi0 = tri[0 + 3*ti];
232 int pil = tri[1 + 3*ti];
233 int pi2 = tri[2 + 3*ti];

```

```

234     if (!(pi0 == pi1 && pi1 == pi2)) { // not a fake triangle
235         vec3 pw0 = ipos[pi0];
236         vec3 pw1 = ipos[pi1];
237         vec3 pw2 = ipos[pi2];
238         vec3 pwm = (pw0 + pw1 + pw2)/3;
239         vec3 nwm = snorm(pwm);
240         vec3 toeye = normalize(camEye - pwm);
241         if (!snsign || toeye•nwm > 0) {
242             vec3 ps0 = unh(CtoS•VtoC•WtoV•hom(lerp(pwm,pw0,0.5)));
243             vec3 ps1 = unh(CtoS•VtoC•WtoV•hom(lerp(pwm,pw1,0.5)));
244             vec3 ps2 = unh(CtoS•VtoC•WtoV•hom(lerp(pwm,pw2,0.5)));
245             real ez = min(min(ps0[2], ps1[2]), ps2[2]);
246             if (-1 <= ez && ez <= 1 && trigray <= 1) {
247                 print(ez, " pop ");
248                 print(trigray, " setgray ",
249                     ps0[0], " ", ps0[1], " moveto ",
250                     ps1[0], " ", ps1[1], " lineto ",
251                     ps2[0], " ", ps2[1],
252                     " lineto closepath fill % ti=", ti, "\n");
253             }
254         }
255     }
256 }
257 if (ii == (pntNum+edgNum+triNum)-1) {
258     print("-2 pop ");
259     print("grestore grestore\n");
260 }
261 stabilize;
262 }
263 }
264
265 initially { draw(ii) | ii in 0 .. (pntNum+edgNum+triNum)-1 };

```